Search for anomalous production of di-lepton events with missing transverse momentum in e$^+$e$^-$ collisions at $\sqrt{s} = 161$ and 172 GeV

The OPAL Collaboration

K. Ackerstaff[8], G. Alexander[23], J. Allison[16], N. Altekamp[5], K.J. Anderson[9], S. Anderson[12], S. Arcelli[2], S. Asai[24], D. Axen[29], G. Azuelos[18,a], A.H. Ball[17], E. Barberio[8], R.J. Barlow[16], R. Bartoldus[3], J.R. Batley[5], S. Baumann[3], J. Bechtluft[14], C. Beeston[16], T. Behnke[8], A.N. Bell[1], K.W. Bell[20], G. Bella[23], S. Bentvelsen[8], S. Bethke[14], O. Biebel[14], A. Biguzzi[5], S.D. Bird[16], V. Blobel[27], I.J. Bloodworth[1], J.E. Bloomer[1], M. Bobinski[10], P. Bock[11], D. Bonacorsi[2], M. Boutemeur[34], B.T. Bouwens[12], S. Braibant[12], L. Brigliadori[2], R.M. Brown[20], H.J. Burckhart[8], C. Burgard[8], R. Bürgin[10], P. Capiluppi[2], R.K. Carnegie[6], A.A. Carter[13], J.R. Carter[5], C.Y. Chang[17], D.G. Charlton[1,b], D. Chrisman[4], P.E.L. Clarke[15], I. Cohen[23], J.E. Conboy[15], O.C. Cooke[8], M. Cuffiani[2], S. Dado[22], C. Dallapiccola[17], G.M. Dallavalle[2], R. Davis[30], S. De Jong[12], L.A. del Pozo[4], K. Desch[3], B. Dienes[33,d], M.S. Dixit[7], E. do Couto e Silva[12], M. Doucet[18], E. Duchovni[26], G. Duckeck[34], I.P. Duerdoth[16], D. Eatough[16], J.E.G. Edwards[16], P.G. Estabrooks[6], H.G. Evans[9], M. Evans[13], F. Fabbri[2], M. Fanti[2], A.A. Faust[30], F. Fiedler[27], M. Fierro[2], H.M. Fischer[3], I. Fleck[8], R. Folman[26], D.G. Fong[17], M. Foucher[17], A. Fürtjes[8], D.I. Futyan[16], P. Gagnon[7], J.W. Gary[4], J. Gascon[18], S.M. Gascon-Shotkin[17], N.I. Geddes[20], C. Geich-Gimbel[3], T. Geralis[20], G. Giacomelli[2], P. Giacomelli[4], R. Giacomelli[2], V. Gibson[5], W.R. Gibson[13], D.M. Gingrich[30,a], D. Glenzinski[9], J. Goldberg[22], M.J. Goodrick[5], W. Gorn[4], C. Grandi[2], E. Gross[26], J. Grunhaus[23], M. Gruwé[8], C. Hajdu[32], G.G. Hanson[12], M. Hansroul[8], M. Hapke[13], C.K. Hargrove[7], P.A. Hart[9], C. Hartmann[3], M. Hauschild[8], C.M. Hawkes[5], R. Hawkings[27], R.J. Hemingway[6], M. Herndon[17], G. Herten[10], R.D. Heuer[8], M.D. Hildreth[8], J.C. Hill[5], S.J. Hillier[1], P.R. Hobson[25], R.J. Homer[1], A.K. Honma[28,a], D. Horváth[32,c], K.R. Hossain[30], R. Howard[29], P. Hüntemeyer[27], D.E. Hutchcroft[5], P. Igo-Kemenes[11], D.C. Imrie[25], M.R. Ingram[16], K. Ishii[24], A. Jawahery[17], P.W. Jeffreys[20], H. Jeremie[18], M. Jimack[1], A. Joly[18], C.R. Jones[5], G. Jones[16], M. Jones[6], U. Jost[11], P. Jovanovic[1], T.R. Junk[8], D. Karlen[6], V. Kartvelishvili[16], K. Kawagoe[24], T. Kawamoto[24], P.I. Kayal[30], R.K. Keeler[28], R.G. Kellogg[17], B.W. Kennedy[20], J. Kirk[29], A. Klier[26], S. Kluth[8], T. Kobayashi[24], M. Kobel[10], D.S. Koetke[6], T.P. Kokott[3], M. Kolrep[10], S. Komamiya[24], T. Kress[11], P. Krieger[6], J. von Krogh[11], P. Kyberd[13], G.D. Lafferty[16], R. Lahmann[17], W.P. Lai[19], D. Lanske[14], J. Lauber[15], S.R. Lautenschlager[31], J.G. Layter[4], D. Lazic[22], A.M. Lee[31], E. Lefebvre[18], D. Lellouch[26], J. Letts[12], L. Levinson[26], S.L. Lloyd[13], F.K. Loebinger[16], G.D. Long[28], M.J. Losty[7], J. Ludwig[10], A. Macchiolo[2], A. Macpherson[30], M. Mannelli[8], S. Marcellini[2], C. Markus[3], A.J. Martin[13], J.P. Martin[18], G. Martinez[17], T. Mashimo[24], P. Mättig[3], W.J. McDonald[30], J. McKenna[29], E.A. Mckigney[15], T.J. McMahon[1], R.A. McPherson[8], F. Meijers[8], S. Menke[3], F.S. Merritt[9], H. Mes[7], J. Meyer[27], A. Michelini[2], G. Mikenberg[26], D.J. Miller[15], A. Mincer[22,e], R. Mir[26], W. Mohr[10], A. Montanari[2], T. Mori[24], M. Morii[24], U. Müller[3], S. Mihara[24], K. Nagai[26], I. Nakamura[24], H.A. Neal[8], B. Nellen[3], R. Nisius[8], S.W. O'Neale[1], F.G. Oakham[7], F. Odorici[2], H.O. Ogren[12], A. Oh[27], N.J. Oldershaw[16], M.J. Oreglia[9], S. Orito[24], J. Pálinkás[33,d], G. Pásztor[32], J.R. Pater[16], G.N. Patrick[20], J. Patt[10], M.J. Pearce[1], R. Perez-Ochoa[8], S. Petzold[27], P. Pfeifenschneider[14], J.E. Pilcher[9], J. Pinfold[30], D.E. Plane[8], P. Poffenberger[28], B. Poli[2], A. Posthaus[3], D.L. Rees[1], D. Rigby[1], S. Robertson[28], S.A. Robins[22], N. Rodning[30], J.M. Roney[28], A. Rooke[15], E. Ros[8], A.M. Rossi[2], P. Routenburg[30], Y. Rozen[22], K. Runge[10], O. Runolfsson[8], U. Ruppel[14], D.R. Rust[12], R. Rylko[25], K. Sachs[10], T. Saeki[24], E.K.G. Sarkisyan[23], C. Sbarra[29], A.D. Schaile[34], O. Schaile[34], F. Scharf[3], P. Scharff-Hansen[8], P. Schenk[34], J. Schieck[11], P. Schleper[11], B. Schmitt[8], S. Schmitt[11], A. Schöning[8], M. Schröder[8], H.C. Schultz-Coulon[10], M. Schumacher[3], C. Schwick[8], W.G. Scott[20], T.G. Shears[16], B.C. Shen[4], C.H. Shepherd-Themistocleous[8], P. Sherwood[15], G.P. Siroli[2], A. Sittler[27], A. Skillman[15], A. Skuja[17], A.M. Smith[8], G.A. Snow[17], R. Sobie[28], S. Söldner-Rembold[10], R.W. Springer[30], M. Sproston[20], K. Stephens[16], J. Steuerer[27], B. Stockhausen[3], K. Stoll[10], D. Strom[19], P. Szymanski[20], R. Tafirout[18], S.D. Talbot[1], S. Tanaka[24], P. Taras[18], S. Tarem[22], R. Teuscher[8], M. Thiergen[10], M.A. Thomson[8], E. von Törne[3], S. Towers[6], I. Trigger[18], Z. Trócsányi[33], E. Tsur[23], A.S. Turcot[9], M.F. Turner-Watson[8], P. Utzat[11], R. Van Kooten[12], M. Verzocchi[10], P. Vikas[18], E.H. Vokurka[16], H. Voss[3], F. Wäckerle[10], A. Wagner[27], C.P. Ward[5], D.R. Ward[5], P.M. Watkins[1], A.T. Watson[1], N.K. Watson[1], P.S. Wells[8], N. Wermes[3], J.S. White[28], B. Wilkens[10], G.W. Wilson[27], J.A. Wilson[1], G. Wolf[26], T.R. Wyatt[16], S. Yamashita[24], G. Yekutieli[26], V. Zacek[18], D. Zer-Zion[8]

[1] School of Physics and Space Research, University of Birmingham, Birmingham B15 2TT, UK
[2] Dipartimento di Fisica dell' Università di Bologna and INFN, I-40126 Bologna, Italy
[3] Physikalisches Institut, Universität Bonn, D-53115 Bonn, Germany

[4] Department of Physics, University of California, Riverside CA 92521, USA
[5] Cavendish Laboratory, Cambridge CB3 0HE, UK
[6] Ottawa-Carleton Institute for Physics, Department of Physics, Carleton University, Ottawa, Ontario K1S 5B6, Canada
[7] Centre for Research in Particle Physics, Carleton University, Ottawa, Ontario K1S 5B6, Canada
[8] CERN, European Organisation for Particle Physics, CH-1211 Geneva 23, Switzerland
[9] Enrico Fermi Institute and Department of Physics, University of Chicago, Chicago IL 60637, USA
[10] Fakultät für Physik, Albert Ludwigs Universität, D-79104 Freiburg, Germany
[11] Physikalisches Institut, Universität Heidelberg, D-69120 Heidelberg, Germany
[12] Indiana University, Department of Physics, Swain Hall West 117, Bloomington IN 47405, USA
[13] Queen Mary and Westfield College, University of London, London E1 4NS, UK
[14] Technische Hochschule Aachen, III Physikalisches Institut, Sommerfeldstrasse 26-28, D-52056 Aachen, Germany
[15] University College London, London WC1E 6BT, UK
[16] Department of Physics, Schuster Laboratory, The University, Manchester M13 9PL, UK
[17] Department of Physics, University of Maryland, College Park, MD 20742, USA
[18] Laboratoire de Physique Nucléaire, Université de Montréal, Montréal, Quebec H3C 3J7, Canada
[19] University of Oregon, Department of Physics, Eugene OR 97403, USA
[20] Rutherford Appleton Laboratory, Chilton, Didcot, Oxfordshire OX11 0QX, UK
[22] Department of Physics, Technion-Israel Institute of Technology, Haifa 32000, Israel
[23] Department of Physics and Astronomy, Tel Aviv University, Tel Aviv 69978, Israel
[24] International Centre for Elementary Particle Physics and Department of Physics, University of Tokyo, Tokyo 113, and Kobe University, Kobe 657, Japan
[25] Brunel University, Uxbridge, Middlesex UB8 3PH, UK
[26] Particle Physics Department, Weizmann Institute of Science, Rehovot 76100, Israel
[27] Universität Hamburg/DESY, II Institut für Experimental Physik, Notkestrasse 85, D-22607 Hamburg, Germany
[28] University of Victoria, Department of Physics, P O Box 3055, Victoria BC V8W 3P6, Canada
[29] University of British Columbia, Department of Physics, Vancouver BC V6T 1Z1, Canada
[30] University of Alberta, Department of Physics, Edmonton AB T6G 2J1, Canada
[31] Duke University, Dept of Physics, Durham, NC 27708-0305, USA
[32] Research Institute for Particle and Nuclear Physics, H-1525 Budapest, P O Box 49, Hungary
[33] Institute of Nuclear Research, H-4001 Debrecen, P O Box 51, Hungary
[34] Ludwigs-Maximilians-Universität München, Sektion Physik, Am Coulombwall 1, D-85748 Garching, Germany

Abstract. Events containing two charged leptons and significant missing transverse momentum are selected from a data sample corresponding to a total integrated luminosity of 20.6 pb^{-1} at centre-of-mass energies of 161 GeV and 172 GeV. The observed number of events, four at 161 GeV and nine at 172 GeV, is consistent with the number expected from Standard Model processes, predominantly arising from W^+W^- production with each W decaying leptonically. This topology is also an experimental signature for the pair production of new particles that decay to a charged lepton accompanied by one or more invisible particles. Further event selection criteria are described that optimise the sensitivity to particular new physics channels. No evidence for new phenomena is observed and limits on the production of scalar charged lepton pairs and other new particles are presented.

1 Introduction

We report on the selection of events containing two charged leptons and significant missing transverse momentum. We give the results of searches for several anomalous sources of such events at centre-of-mass energies of 161 and 172 GeV.

A number of Standard Model processes can lead to the $\ell^+\nu\,\ell^-\overline{\nu}$ final state. Here ℓ represents e, μ or τ and the two charged leptons may be of the same or differ-

---

[a] and at TRIUMF, Vancouver, Canada V6T 2A3

[b] and Royal Society University Research Fellow

[c] and Institute of Nuclear Research, Debrecen, Hungary

[d] and Department of Experimental Physics, Lajos Kossuth University, Debrecen, Hungary

[e] and Department of Physics, New York University, NY 1003, USA

ent flavour. The most common source is expected to be W^+W^- production in which both W's decay leptonically: $W^- \to \ell^-\overline{\nu}_\ell$.

This topology is also an experimental signature for the production of new particles that result in final states with two charged leptons accompanied by one or more invisible particles. Such invisible particles can be weakly interacting particles such as neutrinos or the hypothesised lightest stable supersymmetric [1] particle (LSP), which may be the lightest neutralino, $\tilde{\chi}_1^0$, or the gravitino. Experimentally, invisible particles may also be weakly interacting neutral particles with long lifetimes, which decay outside the detector volume.

One example of a new physics possibility for which this topology is an experimental signature is the pair produc-

tion of charged scalar leptons (sleptons, $\tilde{\ell}^{\pm}$) in the framework of supersymmetry:

$$e^+e^- \rightarrow \tilde{\ell}^+ \tilde{\ell}^-,$$
$$\tilde{\ell}^{\pm} \rightarrow \ell^{\pm} \tilde{\chi}_1^0,$$

where $\ell^{\pm}$ is the corresponding charged lepton. We present searches for scalar electrons (selectrons, $\tilde{e}$), scalar muons (smuons, $\tilde{\mu}$) and scalar taus (staus, $\tilde{\tau}$). If the gravitino were the LSP and if the slepton were to decay to lepton-gravitino the same experimental signature would be produced.

Models with extended Higgs sectors predict the existence of several new Higgs particles, including at least one pair of charged Higgs particles. The pair production of charged Higgs can lead to di-tau events from the decay $H^{\pm} \rightarrow \tau^{\pm} \nu_{\tau}$.

Di-lepton events with missing transverse momentum is a signature also for chargino pair production when both charginos decay to produce a charged lepton and invisible particles:

$$e^+e^- \rightarrow \tilde{\chi}_1^+ \tilde{\chi}_1^-,$$
$$\tilde{\chi}_1^{\pm} \rightarrow \ell^{\pm} \tilde{\nu}_{\ell} \quad \text{or} \quad \tilde{\chi}_1^{\pm} \rightarrow \ell^{\pm} \nu_{\ell} \tilde{\chi}_1^0,$$

where $\tilde{\nu}_{\ell}$ is a scalar neutrino (sneutrino). The $\tilde{\chi}_1^{\pm}$ decay to the final state $\ell^{\pm} \nu_{\ell} \tilde{\chi}_1^0$ may take place via an intermediate, real or virtual, W or charged slepton or sneutrino. If the $\tilde{\chi}_1^{\pm}$ decay via a W dominates then 90% of the produced events contain quarks in the final state; for this case limits are given in [2,3]. However, if one or more sneutrinos or charged sleptons are light then final states containing a pair of charged leptons and invisible particles may dominate, in which case the search presented in this paper is more sensitive.

The detailed properties of the expected events (e.g., the type of leptons observed and their momenta) varies greatly depending on the type of new particles produced and on free parameters within the models. For example, in $\tilde{\ell}^+ \tilde{\ell}^-$ production, if the mass difference Δm between the $\tilde{\ell}$ and $\tilde{\chi}_1^0$ is small, the visible energy and transverse momentum will be small. The main experimental challenge in this case is to detect such "small Δm" events in the presence of the large potential background from two-photon processes, in particular $e^+e^- \rightarrow e^+e^- \ell^+\ell^-$. Conversely, if Δm is large the visible energy and transverse momentum will be large and the new physics events may be difficult to distinguish from W^+W^- events.

The event selection is performed in two stages. The first stage consists of a general selection for all the possible events containing a lepton pair plus genuine missing transverse momentum (Sect. 3.1). In this context the Standard Model $\ell^+ \nu \ell^- \overline{\nu}$ events are considered as signal in addition to the possible new physics sources. All Standard Model processes that do not lead to $\ell^+ \nu \ell^- \overline{\nu}$ final states — e.g., $e^+e^- \ell^+\ell^-$ and $\ell^+\ell^-(\gamma)$ — are considered as background and are reduced to a rather low level in this selection. In the second stage the detailed properties of the events are used to separate as far as possible the events consistent with potential new physics sources from W^+W^- and other Standard Model processes (Sect. 4).

The number and properties of the observed events are found to be consistent with the expectations for Standard Model processes (Sect. 5). We present limits on the production of charged scalar leptons, leptonically decaying charged Higgs and charginos that decay to produce a charged lepton and invisible particles (Sect. 6). In a companion paper [4] we use the same event selections to measure the production of $W^+W^- \rightarrow \ell^+ \nu \ell^- \overline{\nu}$ events.

2 OPAL detector and Monte Carlo simulation

A complete description of the OPAL detector[1] can be found elsewhere [5]. Subdetectors relevant to the current analyses are described very briefly here.

The central detector consists of a system of tracking chambers providing charged particle tracking over 96% of the full solid angle inside a 0.435 T uniform magnetic field parallel to the beam axis. It consists of a two-layer silicon microstrip vertex detector, a high precision drift chamber (CV), a large volume jet chamber (CJ) and a set of z chambers (CZ) that measure the track coordinates along the beam direction.

A lead-glass electromagnetic calorimeter (ECAL) located outside the magnet coil covers the full azimuthal range with excellent hermeticity in the polar angle range of $|\cos\theta| < 0.82$ for the barrel region (EB) and $0.81 < |\cos\theta| < 0.984$ for the endcap region (EE). Electromagnetic calorimeters close to the beam axis complete the geometrical acceptance down to approximately 25 mrad. These include the forward detectors (FD) which are lead-scintillator sandwich calorimeters and, at smaller angles, silicon tungsten calorimeters (SW) located on both sides of the interaction point. The gap between the EE and FD calorimeters is instrumented with an additional lead-scintillator electromagnetic calorimeter, called the gamma-catcher (GC).

The magnet return yoke is instrumented for hadron calorimetry (HCAL) and consists of barrel and endcap sections along with pole tip detectors that together cover the region $|\cos\theta| < 0.99$. Outside the hadron calorimeter, four layers of muon chambers cover the polar angle range of $|\cos\theta| < 0.98$.

The following Standard Model processes are simulated. 4-fermion production is generated using grc4f [6], PYTHIA [7] and EXCALIBUR [8]. Two-photon processes are generated using the program of Vermaseren [9] for $e^+e^- \ell^+\ell^-$, and using PHOJET [10] and PYTHIA for $e^+e^- q\overline{q}$. For the generation of the $e^+e^- e^+e^-$ events it is required that the mass of the two-photon system exceeds 0.2 GeV, and similarly for the $e^+e^- q\overline{q}$ events this mass is required to exceed 2 GeV. For the $e^+e^- e^+e^-$ and $e^+e^- \mu^+\mu^-$ events it is also required that at least one lepton satisfies $|\cos\theta| < 0.975$ and $p_t > 1$ GeV. No cuts are applied to the $e^+e^- \tau^+\tau^-$ generation. The production of lepton pairs is generated

---

[1] A right-handed coordinate system is adopted, in which the x-axis points to the centre of the LEP ring, and positive z is along the electron beam direction. The angles θ and ϕ are the polar and azimuthal angles, respectively

using Bhwide [11] and Teegg [12] for $e^+e^-(\gamma)$, and using Koralz [13] for $\mu^+\mu^-(\gamma)$ and $\tau^+\tau^-(\gamma)$. The production of quark pairs, $q\bar{q}(g)$, is generated using Pythia and the final state $\nu\bar{\nu}\gamma\gamma$ is generated using Nunugpv [14] and Koralz.

The following new physics processes are simulated. Slepton pair production is generated using Susygen [15]. Charged Higgs pair production is generated using Pythia. Chargino pair production is generated using Susygen and Pythia. All Standard Model and new physics Monte Carlo samples are processed with a full simulation of the OPAL detector [16] and subjected to the same reconstruction and analysis programs as used for the OPAL data.

3 Selection of di-lepton events with significant missing momentum

3.1 General selection

The first stage in the analysis consists of a general selection for all the possible events containing a lepton pair plus genuine missing transverse momentum. At this stage Standard Model $\ell^+\nu\ell^-\bar{\nu}$ events are considered as signal in addition to the possible new physics sources. In this section we give a general overview of the selection; details are given in the appendices.

The event selection requires evidence that a pair of leptons is produced in association with an invisible system that carries away significant missing energy and momentum. A number of additional cuts are applied to distinguish events with genuine prompt missing momentum (Standard Model $\ell^+\nu\ell^-\bar{\nu}$ events and potential new physics) from the background, in which the signature of missing momentum is faked by Standard Model processes containing, e.g., secondary neutrinos from tau decays or particles that strike regions of the detector where they are undetected or poorly measured.

Leptons may be identified as electrons, muons or hadronically decaying taus[2]. The flavour of the two lepton candidates is not required to be the same.

A number of Standard Model processes can lead to high energy particles travelling down the beam pipe, thus being undetected and giving rise to missing momentum along the beam axis. Therefore, in selecting candidate signal events we require a significant missing momentum in the plane perpendicular to the beam axis (p_t^{miss}) and require that the total missing momentum vector points away from the beam axis. Nevertheless, Standard Model events containing neutrinos (in particular from tau decay) or poorly measured particles represent a potential background to this signature. In these events the value of p_t^{miss} may be large and the missing momentum vector may point at a large angle to the beam axis; such events may thus survive cuts on these quantities. However, in the majority of Standard Model events the two leptons

tend to be approximately back-to-back in the plane perpendicular to the beam axis (coplanar). In coplanar events the component of p_t^{miss} that is perpendicular to the event thrust axis in the transverse plane, which is referred to as a_t^{miss}, is much less sensitive than p_t^{miss} to the presence of neutrinos from tau decays or poorly measured particles. A cut on a_t^{miss} is also more performant than a cut on the acoplanarity angle[3], ϕ_{acop}. Consider, for example, electrons produced in tau decay. Low momentum electrons from this source may be produced at very large angles to the original tau direction (thus causing a large ϕ_{acop}), but their momentum transverse to the original tau direction (and thus their contribution to a_t^{miss}) is small. In events that are relatively coplanar a cut on a_t^{miss} is applied and the direction of the missing momentum vector is calculated using a_t^{miss} rather than p_t^{miss}. At large acoplanarity cuts using a_t^{miss} no longer discriminate sufficiently between signal and background and a hard cut on p_t^{miss} and a conventional cut on the direction of the missing momentum are made.

The dominant background that survives cuts on missing momentum arises from two-photon lepton pairs in which one of the initial state beam particles is scattered at an appreciable angle to the beam direction. Events that may have arisen from such processes are suppressed by requiring no significant energy to be present in the GC, FD and SW detectors.

Muons and hadrons produced at small angles to the beam direction ($\theta < 0.2$ rad) are likely to be poorly measured in the detector. In order to reduce the Standard Model background from events containing such particles, the muon chambers, hadron calorimeters and central detector are examined for any evidence of particles escaping in the very forward region that might fake the signature of missing momentum.

Two independently developed selections are used in the first stage general selection of acoplanar di-lepton events. In one selection particular emphasis has been placed on retaining efficiency for events with very low visible energy, but nevertheless significant missing transverse momentum. It is referred to below as "selection I" and is described in detail in Appendix I of this paper. An earlier version of this selection has been used to set limits on new particle production at $\sqrt{s} = 130$–136 GeV [17]. A second selection has been optimised to select and measure the rate of high visible energy events such as those from W^+W^- events in which both W's decay leptonically. It is referred to below as "selection II" and is described in detail in Appendix II. An earlier version of this selection has been used at $\sqrt{s} = 161$ GeV to measure the production of $W^+W^- \to \ell^+\nu\ell^-\bar{\nu}$ events [18].

For events with high visible energy such as W^+W^- or in new physics scenarios with large mass differences betweeen the parent and the visible daughter particles, the two selections have similar efficiency and background acceptance. However, a significant fraction of the Monte

---

[2] Leptonically decaying taus are normally identified as isolated electrons or muons

[3] The acoplanarity angle (ϕ_{acop}) is defined as the supplement of the angle between the two lepton candidates in the plane transverse to the beam direction

Carlo signal events are selected exclusively by only one of the two selections. The general selection of acoplanar di-lepton events is, therefore, defined as the logical ".or." of the selections "I" and "II".

The general selection of acoplanar di-lepton events has been applied to the data at centre-of-mass energies of 161 and 172 GeV. Four candidate events are selected at 161 GeV. The total number of selected events predicted by the Standard Model Monte Carlo for the integrated luminosity[4] of 10.3 pb^{-1} is 4.7 ± 0.3 (stat) events, of which 3.5 events arise from 4-fermion processes with genuine prompt missing energy and momentum ($\ell^+ \nu \ell^- \overline{\nu}$) and 1.2 events are background coming mainly from processes with four charged leptons in the final state (of which only two are observed in the detector). About half of the e$^+$e$^- \ell^+ \ell^-$ background arises from two-photon (multiperipheral) processes and about half from other four-fermion processes, most notably e$^+$e$^-$Z$^*/\gamma^* \rightarrow$ e$^+$e$^- \mu^+ \mu^-$.

Nine candidate events are selected at 172 GeV. The total number of selected events predicted by the Standard Model Monte Carlo for the integrated luminosity of 10.3 pb^{-1} is 12.1 ± 0.3 (stat) events, of which 11.0 events arise from $\ell^+ \nu \ell^- \overline{\nu}$ and 1.1 events do not have genuine missing momentum.

The properties of the four events selected at $\sqrt{s} = 161$ GeV are given in Table 1. The properties of the nine events selected at $\sqrt{s} = 172$ GeV are given in Table 2. Event displays of two of the candidates at $\sqrt{s} = 172$ GeV are shown in Figs. 1 and 2.

In Fig. 3 the selected candidates at $\sqrt{s} = 161$ GeV are plotted in the (x_{max}, x_{min}) plane. The scaled momenta of the lepton candidates are defined by:

$$x_{max} = \frac{p_{max}}{E_{beam}}, \quad x_{min} = \frac{p_{min}}{E_{beam}},$$

where p_{max} is the momentum of the higher momentum lepton, and p_{min} is the momentum of the lower momentum lepton. The Standard Model Monte Carlo distribution in the (x_{max}, x_{min}) plane is also shown in Fig. 3. Because the W's are produced approximately at rest, electrons and muons from W decays, W $\rightarrow$ eν and W $\rightarrow \mu\nu$, have a momentum close to half the beam energy. This is seen in the clustering of events with x_{min} and x_{max} close to 0.5. In general, the process W $\rightarrow \tau\nu$ produces lepton candidates with lower values of scaled momentum than those produced in W $\rightarrow$ eν and W $\rightarrow \mu\nu$ decays. The clustering of events at very low x_{max} and x_{min} results mainly from the e$^+$e$^- \ell^+ \ell^-$ background. The Monte Carlo at $\sqrt{s} = 172$ GeV (Fig. 4) shows a W$^+$W$^-$ peak that is broader than at $\sqrt{s} = 161$ GeV, because the W's are no longer at rest.

The lepton identification information in the selected data events is compared with the Standard Model expectation in Table 3. The numbers of events observed in the data are consistent with Standard Model expectations. Of particular interest are the numbers of events in which the flavour of the two observed leptons is the same. In

---

Table 1. Properties of the selected events at 161 GeV. The row labelled "Lepton id." gives the results of the lepton identification; "h" means that the lepton is identified neither as an electron nor muon and so is probably the product of a hadronic tau decay. Leptonic decays of taus are usually classified as electron or muon. The "W$^+$W$^-$ classification" row indicates whether ("Y") or not ("N") the event is selected as a W$^+$W$^-$ candidate as defined in Sect. 3.2. The row labelled "Candidate for:" is relevant to the new particle searches described in Sect. 4 below. It gives the new physics categories for which a given event is selected as a candidate. A dash "–" indicates that an event is not consistent with any new physics category according to the cuts of Sect. 4. x_+ and x_- are the momenta of the positively charged lepton and negatively charged lepton, respectively, as a fraction of the beam energy. $m_{\ell\ell}$ and m_{recoil} are the invariant masses of the lepton pair and of the invisible particles, respectively

	Candidate			
	1	2	3	4
Run Number	7270	7274	7402	7463
Event Number	9719	61080	203918	62162
Selection	I	I,II	I,II	I
Lepton id.	h^+h^-	$\mu^+\mu^-$	e$^-\mu^+$	e$^+h^-$
W$^+$W$^-$ classification	Y	Y	Y	N
Candidate for:	$\tilde{\tau}$,H,$\tilde{\chi}$	$\tilde{\mu}$,$\tilde{\chi}$	–	$\tilde{e}$,$\tilde{\tau}$,$\tilde{\chi}$
ϕ_{acop} (rad)	2.31	0.50	0.43	3.06
$p_t^{\mathrm{miss}}/E_{\mathrm{beam}}$	0.14	0.27	0.19	0.05
x_+	0.15	0.63	0.55	0.07
x_-	0.21	0.28	0.56	0.01
$m_{\ell\ell}$ (GeV)	22.1	64.9	87.7	2.0
m_{recoil} (GeV)	136.1	81.2	69.1	154.4

W$^+$W$^- \rightarrow \ell^+ \nu \ell^- \overline{\nu}$ events there is no correlation between the flavour of the two leptons. Some new physics sources of acoplanar di-leptons would produce events with correlated lepton flavour, for example, the pair production of sleptons or charged Higgs.

The event classes e$^+$e$^-$, $\mu^+\mu^-$ and e$^\pm\mu^\mp$ receive a large contribution from W$^+$W$^-$. In order to increase the potential sensitivity to new physics sources of events in these categories whilst minimising the assumptions we have to make about the kinematics of any new physics events, we can remove events in which both leptons have momentum in the region expected for prompt W $\rightarrow$ eν and W $\rightarrow \mu\nu$ decays. We remove events in which both leptons have $0.40 < p/E_{\mathrm{beam}} < 0.65$ at $\sqrt{s} = 161$ GeV and $0.36 < p/E_{\mathrm{beam}} < 0.68$ at $\sqrt{s} = 172$ GeV. As can be seen in Figs. 3 and 4 these regions contain a large fraction of the expected W$^+$W$^-$ events. The results are shown in the final three rows of Table 3. There is no indication of an excess in the data with respect to the Standard Model expectations in any category. In the following sections we will apply more sophisticated selections in order to optimise the sensitivity to various potential new physics sources of acoplanar di-lepton events.

Figure 5 shows the distributions of **a** $m_{\ell\ell}$ and **b** $p_t^{\mathrm{miss}}/E_{\mathrm{beam}}$ of the observed events at $\sqrt{s} = 172$ GeV compared
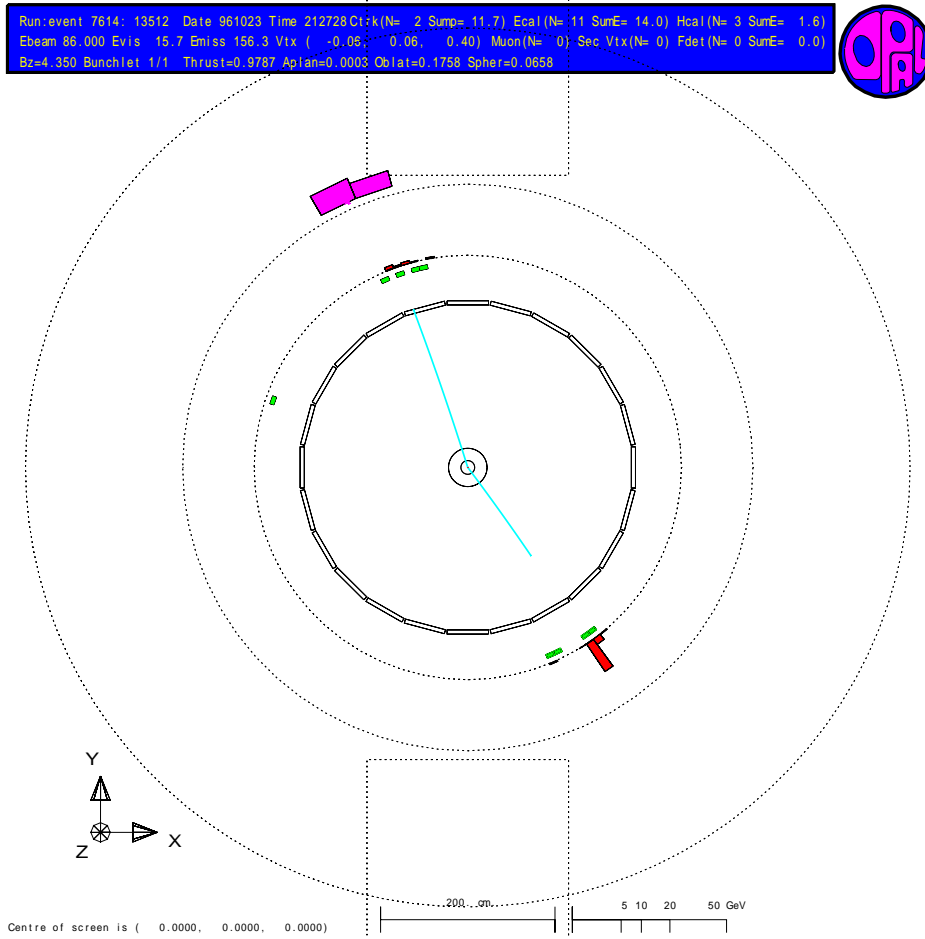
```
Run:event 7614: 13512  Date 961023 Time 212728 Ctrk(N=  2 Sump= 11.7) Ecal(N= 11 SumE= 14.0) Hcal(N= 3 SumE=  1.6)
Ebeam 86.000 Evis  15.7 Emiss 156.3 Vtx (  -0.06,   0.06,   0.40) Muon(N=  0) Sec Vtx(N= 0) Fdet(N= 0 SumE=  0.0)
Bz=4.350 Bunchlet 1/1  Thrust=0.9787 Aplan=0.0003 Oblat=0.1758 Spher=0.0658
```

Y

Z ⊗ ▷ X

Centre of screen is (0.0000,   0.0000,   0.0000)

200 cm   5 10 20   50 GeV

Fig. 1. Acoplanar di-lepton candidate number 3 at 172 GeV. This event is selected as a W^+W^- candidate and is considered as a candidate in the searches for stau pair, charged Higgs pair and chargino pair production

Table 2. Properties of the selected events at 172 GeV

	Candidate								
	1	2	3	4	5	6	7	8	9
Run Number	7596	7596	7614	7631	7631	7660	7718	7729	7757
Event Number	7824	34581	13512	58714	59299	2314	48005	32594	20446
Selection	I,II	I,II	I	I,II	I	I,II	I,II	I,II	I,II
Lepton id.	h^+h^-	e^-h^+	h^+h^-	$e^+\mu^-$	μ^-h^+	e^+e^-	$e^+\mu^-$	$\mu^+\mu^-$	e^+e^-
W^+W^- classification	Y	Y	Y	Y	N	Y	Y	Y	Y
Candidate for:	$\tilde{\tau}$,H,$\tilde{\chi}$	$\tilde{\tau}$,$\tilde{\chi}$	$\tilde{\tau}$,H,$\tilde{\chi}$	$\tilde{\chi}$	$\tilde{\mu}$,$\tilde{\tau}$,$\tilde{\chi}$	$\tilde{e}$	–	–	$\tilde{e}$,$\tilde{\chi}$
ϕ_{acop} (rad)	0.58	0.34	0.34	0.65	3.13	0.71	2.82	2.16	0.25
$p_t^{\mathrm{miss}}/E_{\mathrm{beam}}$	0.27	0.23	0.041	0.38	0.047	0.51	0.71	0.29	0.12
x_+	0.17	0.15	0.17	0.84	0.01	0.79	0.38	0.61	0.55
x_-	0.42	0.38	0.09	0.66	0.04	0.43	0.40	0.04	0.44
$m_{\ell\ell}$ (GeV)	44.2	32.9	17.2	117.0	1.0	95.1	26.2	16.1	76.3
m_{recoil} (GeV)	118.5	127.5	154.2	–	167.7	50.0	84.2	106.4	77.6

with the Standard Model Monte Carlo. The Standard Model Monte Carlo and data are consistent. Additional comparisons between the data and Standard Model Monte Carlo expectations are given in Appendix I.

3.2 Selection of $W^+W^- \to \ell^+\nu\,\ell^-\overline{\nu}$ candidates

Events are considered as W^+W^- candidates if: (i) they pass selection I and the additional W^+W^- selection cri-

teria designed to suppress two-photon background and non-W^+W^- Standard Model $\ell^+\nu\,\ell^-\overline{\nu}$ events as described in Appendix I.4; or (ii) they pass selection II. Eleven of the thirteen events selected at $\sqrt{s} = 161$ GeV and $\sqrt{s} = 172$ GeV satisfy these criteria.

Run:event 7660:   2314   Date 961101 Time 43154 Ctrk(N= 2 Sump= 80.2) Ecal(N= 11 SumE= 96.6) Hcal(N= 0 SumE= 0.0)
Ebeam 86.000 Evis 81.1 Emiss 90.9 Vtx (-0.06,   0.07,   0.43) Muon(N= 0) Sec Vtx(N= 0) Fdet(N= 0 SumE= 0.0)
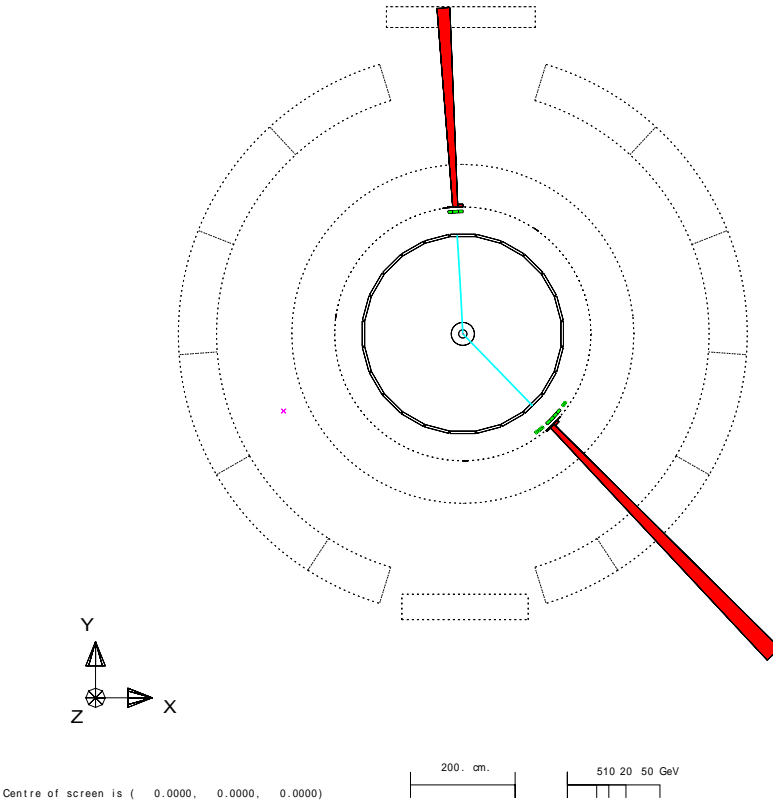Bz=4.350 Bunchlet 1/1 Thrust=0.9695 Aplan=0.0000 Oblat=0.1741 Spher=0.0220

Y

Z ⊗ → X

200. cm.

5 10 20 50 GeV

Centre of screen is (0.0000,   0.0000,   0.0000)

Fig. 2. Acoplanar di-lepton candidate number 6 at 172 GeV. This event is selected as a W^+W^- candidate and is considered as a candidate in the search for selectron pair production

Table 3. Lepton identification information in the selected data events compared with the Standard Model expectation. For further details see the text

Event Class	$\sqrt{s} = 161$ GeV data	SM	$\sqrt{s} = 172$ GeV data	SM
e^+e^-	0	0.6	2	1.7
$\mu^+\mu^-$	1	0.8	1	1.9
$e^\pm\mu^\mp$	1	1.5	2	4.0
$e^\pm h^\mp$	1	0.8	1	2.2
$\mu^\pm h^\mp$	0	0.8	1	1.9
$h^\pm h^\mp$	1	0.2	2	0.4
Apply veto on $W \to e\nu$ and $W \to \mu\nu$ decays				
e^+e^-	0	0.4	1	0.8
$\mu^+\mu^-$	1	0.5	1	1.0
$e^\pm\mu^\mp$	0	1.0	1	2.1

4 Additional selection criteria for specific search channels

4.1 Introduction

Starting from the general selection of acoplanar di-lepton events described in Sect. 3.1, we search for the production of new particles by applying additional cuts to suppress Standard Model sources of such events, the most important of which are $\ell^+\nu\,\ell^-\overline{\nu}$ and $e^+e^-\ell^+\ell^-$.

The Standard Model $\ell^+\nu\,\ell^-\overline{\nu}$ events from W^+W^- are characterised by the production of two leptons, both with p/E_{beam} around 0.5. Equal numbers of $e^\pm$, $\mu^\pm$ and $\tau^\pm$ are produced and there is no correlation between the flavours of the two charged leptons in the event. In the Standard Model $e^+e^-\ell^+\ell^-$ events the two observed leptons both tend to have low momentum.

In the signal events the momentum distribution of the expected leptons varies strongly as a function of the mass difference, Δm between the parent particle (e.g., selectron) and the invisible daughter particle (e.g., lightest neutralino), and, to a lesser extent, m, the mass of the parent particle. When performing a search for a particular new particle at a particular point in m and Δm, an event is considered as a potential candidate only if the results of the lepton identification and the momenta of the observed leptons are consistent with expectations.

In order to maximise the *a priori* potential to discover new physics the additional selection cuts must be tuned to give the optimal balance between signal selection efficiency and the number of selected background events. There is no unique prescription for how to achieve this, particularly when the expected production cross-section and/or branching ratio for new physics channels are unknown,
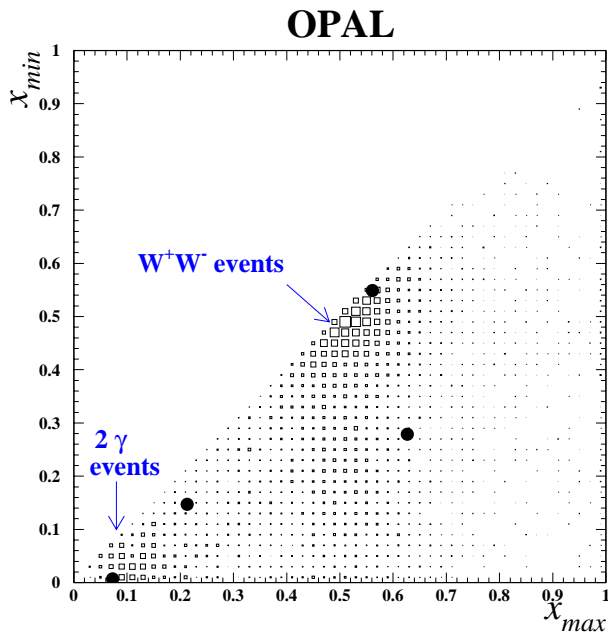
Fig. 3. Distribution in the (x_{max}, x_{min}) plane of events passing the general selection of acoplanar di-leptons at $\sqrt{s} = 161$ GeV. The four data events are shown as the *circular points*. The Standard Model Monte Carlo distribution is shown as the *squares*. The regions that correspond to W^+W^- production and to two-photon processes are indicated
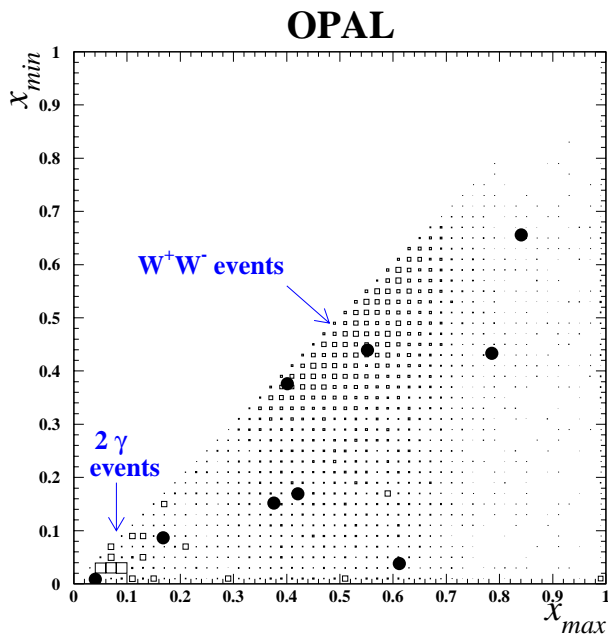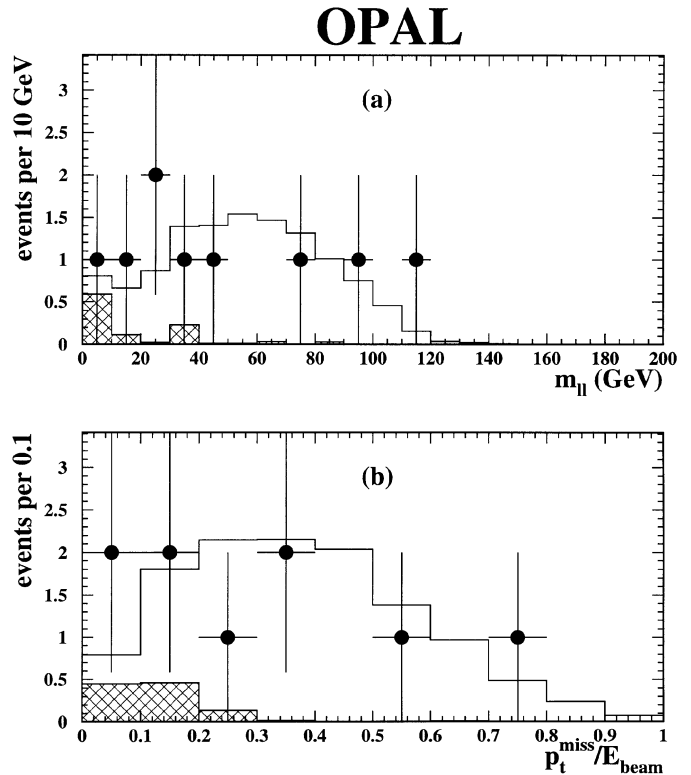

Fig. 4. Distribution in the (x_{max}, x_{min}) plane of events passing the general selection of acoplanar di-leptons at $\sqrt{s} = 172$ GeV. The nine data events are shown as the *circular points*. The Standard Model Monte Carlo distribution is shown as the *squares*. The regions that correspond to W^+W^- production and to two-photon processes are indicated

Fig. 5. Distributions at $\sqrt{s} = 172$ GeV of (a) $m_{\ell\ell}$ and (b) $p_t^{\mathrm{miss}}/E_{\mathrm{beam}}$ of the observed events compared with the Standard Model Monte Carlo. The data are shown as the *points with error bars*. The Monte Carlo prediction for 4-fermion processes with genuine prompt missing energy and momentum ($\ell^+\nu\,\ell^-\overline{\nu}$) is shown as the *open histogram* and the background, coming mainly from processes with four charged leptons in the final state, is shown as the *shaded histogram*

as is the case here. In this analysis we use the following prescription based on the method advocated in [20]. The precise values of the additional selection cuts are chosen in such a way that, in the hypothesis of no signal being present, the *a priori* average value of the 95% CL upper limit on the cross-section for new physics is minimised. This is achieved by an automated optimisation procedure that makes use of Monte Carlo samples of signal and Standard Model backgrounds, but not the experimental data.

4.2 Optimisation of the cut values

For a given set of selection cuts one can estimate μ_B, the mean number of selected Standard Model events expected from Monte Carlo. If N candidate events are actually observed in an experiment, then it is possible to calculate the 95% CL upper limit $N_{95}(N, \mu_B)$ on the expected number of signal events, using the method advocated by the PDG [21].

The upper limit at 95% CL on the cross-section for new particle production is then given by:

$$\sigma_{95} = \frac{N_{95}(N, \mu_B)}{\varepsilon\mathcal{L}},$$

where ε is the selection efficiency for the particular type of new particle production and decay being considered and $\mathcal{L}$ is the integrated luminosity of the experiment.

In the absence of any new physics sources, N is expected to follow a Poisson distribution, $P(N, \mu_B)$, with mean μ_B. We can, therefore, calculate the expectation value of N_{95} for an ensemble of experiments:

$$\langle N_{95}(\mu_B) \rangle = \sum_{N=0}^{\infty} P(N, \mu_B) N_{95}(N, \mu_B).$$

This in turn gives us the expectation value of the 95% CL upper limit on the cross-section for new particle production:

$$\langle \sigma_{95} \rangle = \frac{\langle N_{95}(\mu_B) \rangle}{\varepsilon \mathcal{L}}.$$

A modification to the selection cuts changes both $\langle N_{95}(\mu_B) \rangle$ and ε. An optimised set of cuts is found by minimising $\langle \sigma_{95} \rangle$ using an iterative procedure.

The above can be generalised to include data from more than one $\sqrt{s}$ value. The 95% CL upper limit on the cross-section for new particle production at $\sqrt{s} = 172$ GeV, obtained by combining the data at the two centre-of-mass energies $\sqrt{s} = 161$ GeV and $\sqrt{s} = 172$ GeV is given by:

$$\langle \sigma_{95} \rangle = \frac{\langle N_{95}(\sum_i \mu_{B_i}) \rangle}{\sum_i \varepsilon_i \mathcal{L}_i \omega_i},$$

where the sums run over the two centre-of-mass energies. ω_i is a weight factor which takes into account that the expected production cross-section varies with $\sqrt{s}$, but the limit on the observed cross-section is quoted at $\sqrt{s} = 172$ GeV.

$$\omega_i = \frac{\sigma_i}{\sigma_{172}},$$

where σ_{172} is the expected cross-section for $\sqrt{s} = 172$ GeV and σ_i is the expected cross-section for the i'th value of $\sqrt{s}$. For scalar particles, for example sleptons, we assume that the expected cross-section varies as β^3/s. For spin 1/2 particles, for example charginos, we assume that the expected cross-section varies as β/s.

We can expect the optimal selection cuts to be different at the two centre-of-mass energies, given that we expect different cross-sections at the two centre-of-mass energies, both for signal and background. For example, the W^+W^- cross-section is significantly higher at $\sqrt{s} = 172$ GeV than at $\sqrt{s} = 161$ GeV. In regions of $(m, \Delta m)$ where W^+W^- is the dominant source of background we can expect the optimised selection cuts to be tighter at $\sqrt{s} = 172$ GeV than at $\sqrt{s} = 161$ GeV. The selection cuts at the two centre-of-mass energies are therefore optimised simultaneously. Note that this optimisation of the cut values uses only Monte Carlo signal and background distributions, and thus is not biased by the real data.

4.3 Selection criteria for selectrons

In this section we describe the additional selection criteria in the search for selectron pair production and decay:

$$e^+e^- \to \tilde{e}^+\tilde{e}^-,$$
$$\tilde{e}^\pm \to e^\pm \tilde{\chi}_1^0.$$

In the region of high mass difference, Δm, between $\tilde{e}^\pm$ and $\tilde{\chi}_1^0$ this process would lead to events containing two energetic electrons and the dominant background arises from W pair production:

$$e^+e^- \to W^+W^-,$$
$$W^\pm \to \ell^\pm \nu_\ell.$$

There are two important distinctions between signal and background:

(i) Selectrons always decay to produce electrons, whereas a leptonically decaying W pair decays to $e^+e^-\nu_e\overline{\nu}_e$ with probability of only 1/9.

(ii) $\tilde{\chi}_1^0$ may be massive whereas the neutrino is massless. Therefore electrons from selectron decay will in general be softer than those from W decay. Also the mass of the W is 80 GeV, whereas the mass of the selectron accessible at $\sqrt{s} = 172$ GeV could be anywhere between[5] 45 GeV and 85 GeV, again resulting in different kinematic properties of the observed electrons.

In the region of low Δm, selectron pair production would lead to events containing two low energy electrons and the dominant background arises from $e^+e^-\ell^+\ell^-$ events.

In order to discriminate between selectron pair production and the Standard Model background we make requirements on the results of the lepton identification and on the momenta of the observed leptons.

4.3.1 Kinematic cuts for selectrons

The (x_{max}, x_{min}) distribution expected for the selectron signal varies considerably with the values of m and Δm. The signal Monte Carlo distribution at $\sqrt{s} = 172$ GeV is shown for four different m and Δm values in Fig. 6. As Δm increases, so does the amount of energy available to the electron. As the selectron mass m decreases, the Lorentz boost given to the electrons increases, spreading out the distribution. The signal behaves similarly at $\sqrt{s} = 161$ GeV.

Comparison of the Standard Model background (Fig. 4) and new physics signal (Fig. 6) distributions suggests that two sets of kinematic cuts can be made:

(i) **First stage cuts**: The signal is contained within a triangular region in the (x_{max}, x_{min}) plane. Therefore an upper cut on x_{max} and a lower cut on x_{min} are made.

(ii) **Second stage cuts**: In order to remove the large peak in the background due to W^+W^- production, events within the triangular region containing a large fraction of the W^+W^- are excluded.

The cuts on x_{max}, x_{min} are indicated in Fig. 6. The "second stage" cuts are applied only for those values of m and Δm for which they result in a decrease in $\langle \sigma_{95} \rangle$, calculated using the Monte Carlo events as described in Sect. 4.2.

---

[5] Masses below 45 GeV are not considered given the negative results of searches at LEP1
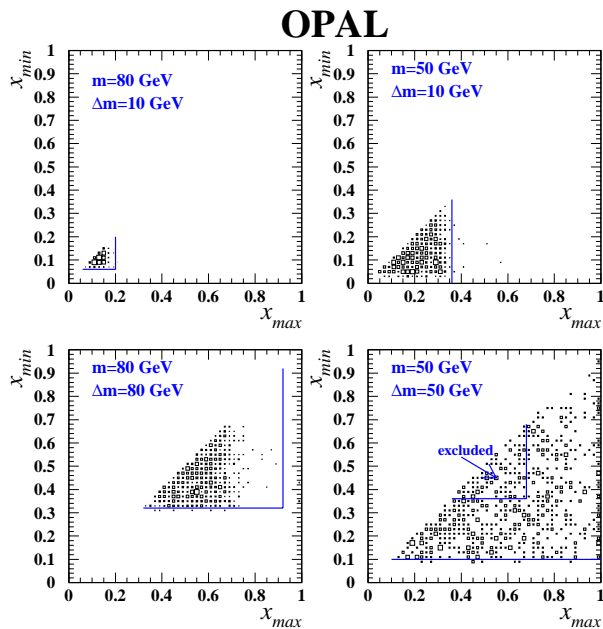
Fig. 6. Selectron Monte Carlo signal distributions in the (x_{max}, x_{min}) plane at $\sqrt{s} = 172$ GeV for four different combinations of $m = m_{\tilde{e}^-}$ and $\Delta m = m_{\tilde{e}^-} - m_{\tilde{\chi}_1^0}$. The kinematic cuts that are applied for these values of m and Δm are indicated

Selectron Monte Carlo samples are available for about 50 different combinations of m and Δm at each centre-of-mass energy. The values of m range from $m = 45$ GeV up to $m \approx E_{\rm beam}$ in 5 GeV steps. For each value of m, the values of Δm range from $\Delta m = 1.5$ GeV up to $\Delta m = m$. There are a total of eight kinematic cut values to be optimised for a given m and Δm (four at each centre-of-mass energy). The available Monte Carlo samples are used to calculate the optimum values of the kinematic cuts for a discrete set of values of m and Δm. The cut values are then parameterised to give cuts that vary continuously as functions of m and Δm. This procedure smoothes out the effect of statistical fluctuations in the individual signal Monte Carlo samples. The validity of the fit is established by verifying that the value of $\langle \sigma_{95} \rangle$ corresponding to the parameterised cuts does not differ significantly from the value corresponding to the optimised cuts.

4.3.2 Lepton identification requirements for selectrons

Although a selectron pair always decays to produce a pair of electrons, it is not necessarily optimal to require that two electrons are identified, as this will result in a loss in efficiency. At each value of $\sqrt{s}$, m and Δm, two possibilities are considered:

(i) require two identified electrons,

or

(ii) require at least one identified electron and no identified muons[6].

We use the combination of lepton type requirements at the two centre-of-mass energies that, after optimisation of the kinematic cuts, gives the lowest value of $\langle \sigma_{95} \rangle$.

It is found that at high values of Δm, where the expected background from W^+W^- is at its highest, $\langle \sigma_{95} \rangle$ is minimised if two electrons are required. Conversely, for low values of Δm, where the efficiency of the general selection is already lower and the expected background from Standard Model processes is also lower, $\langle \sigma_{95} \rangle$ is minimised by requiring one electron and no muons.

4.4 Selection criteria for smuons

The procedure to optimise the selection cuts in the search for smuons is similar to that described for selectrons in Sect. 4.3, except that the two lepton type requirements considered are:

(i) At low Δm: require no identified electrons and at least one identified muon

(ii) At high Δm: require two identified muons.

4.5 Selection criteria for staus

The search for staus is complicated by the fact that the observed particles are the decay products of the taus, rather than the taus themselves:

$$e^+e^- \rightarrow \tilde{\tau}^+\tilde{\tau}^-,$$
$$\tilde{\tau}^\pm \rightarrow \tau^\pm \tilde{\chi}_1^0,$$
$$\tau^\pm \rightarrow e^\pm \nu \bar{\nu} \quad \text{or} \quad \mu^\pm \nu \bar{\nu} \quad \text{or} \quad \text{hadrons} + \nu_\tau.$$

The events are first classified according to the number of identified electrons or muons in the final state. Both W^+W^- and $\tilde{\tau}^+\tilde{\tau}^-$ can decay to final states containing two, one or zero electrons or muons. However, it is important to note that the relative fractions of events in these three classes is very different for W^+W^- and $\tilde{\tau}^+\tilde{\tau}^-$, as is shown in Table 4.

Events containing two identified electrons or muons form a large fraction of the W^+W^- background, but only a small fraction of the $\tau^+\tau^-$ signal. Therefore rather tight cuts on lepton momentum are necessary in this case. This is illustrated in Figs. 7 and 8, which show the distributions in the (x_{min}, x_{max}) plane for events containing two identified electrons or muons. Figure 7 shows the Standard Model expectation and Fig. 8 the simulated $\tilde{\tau}^+\tilde{\tau}^-$ signal for four example m, Δm combinations. The cuts in x_{min} and x_{max} are shown in Fig. 8. It can be seen that the region dominated by W^+W^- events is excluded in all cases. The region in which both observed leptons are soft

---

[6] If the lepton identification fails then the electron track is likely to be identified as a candidate hadronic tau decay. An electron is very unlikely to be identified as a muon candidate. However, a significant fraction of the Standard Model background to the search at low Δm, in particular $e^+e^-\mu^+\mu^-$, contain one observed electron and one observed muon

Table 4. Columns 2 and 3 show the relative fractions of leptonically decaying W^+W^- and $\tilde{\tau}^+\tilde{\tau}^-$ pairs containing two, one or zero $e^\pm$ or $\mu^\pm$ (before selection cuts). Note that in the case of W^+W^- the branching ratio to $e^\pm$ or $\mu^\pm$ includes decays to $e^\pm$ or $\mu^\pm$ via a $\tau^\pm$. Columns 4 and 5 show the number of events in the general selection at $\sqrt{s} = 161$ GeV in these three classes compared with the SM expectation before the cut on the lepton momenta. Columns 6 and 7 show the same information at $\sqrt{s} = 170$–172 GeV

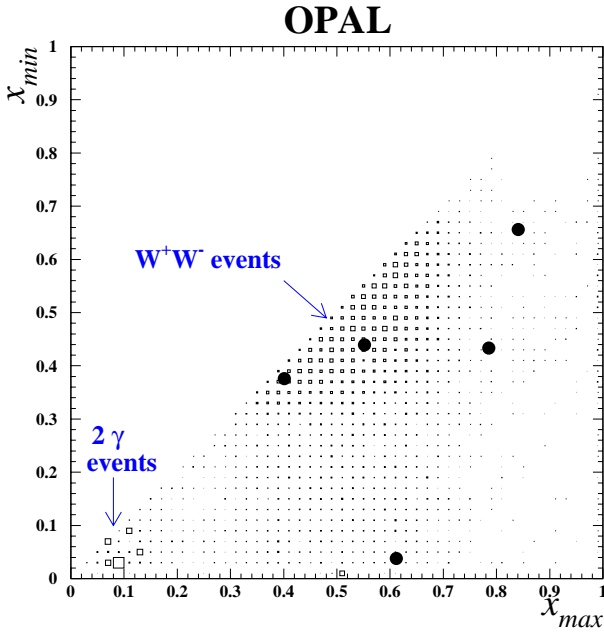| Final State | Fraction | | Number of Events | | | |
| | $W^+W^- \to$ | $\tilde{\tau}^+\tilde{\tau}^- \to$ | $\sqrt{s} = 161$ GeV | | $\sqrt{s} = 172$ GeV | |
	$\ell^+\nu\,\ell^-\overline{\nu}$	$\tau^+\tilde{\chi}_1^0\tau^-\tilde{\chi}_1^0$	data	SM bgrd	data	SM bgrd
e^+e^- or $\mu^+\mu^-$ or $e^\pm\mu^\mp$	0.61	0.12	2	2.9±0.2	5	7.6±0.2
$e^\pm h^\mp$ or $\mu^\pm h^\mp$	0.34	0.46	1	1.6±0.1	2	4.1±0.1
$h^\pm h^\mp$	0.05	0.42	1	0.2±0.0	2	0.4±0.0

Fig. 7. Distribution in the $(x_{max},\ x_{min})$ plane at $\sqrt{s} = 172$ GeV, with the requirement that both the observed leptons are identified as either electrons or muons. The data events are shown as the *circular points*. The Standard Model Monte Carlo distribution is shown as the *squares*. The regions that correspond to W^+W^- production and to two-photon processes are indicated
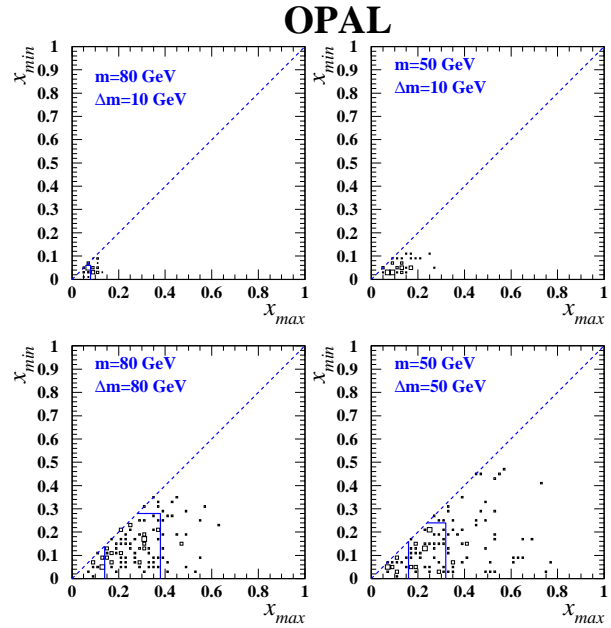

Fig. 8. Stau Monte Carlo signal distribution in the (x_{max}, x_{min}) plane at $\sqrt{s} = 172$ GeV, for four different combinations of $m = m_{\tilde{\tau}^-}$ and $\Delta m = m_{\tilde{\tau}^-} - m_{\tilde{\chi}_1^0}$, with the requirement that both the observed leptons are identified as either electrons or muons. The kinematic cuts that are applied for these values of m and Δm are illustrated. Note that for m=50 GeV, Δm=10 GeV, all events in this class are rejected by the automated cut optimisation procedure; therefore no acceptance box is shown on the figure. For m=80 GeV, Δm=10 GeV, events in the region $x_{max} < 0.08$, $x_{min} < 0.06$ are accepted, although the acceptance box is difficult to see in the figure. For further discussion see Sect. 4.5 and Table 4

is dominated by $e^+e^-\ell^+\ell^-$ events. It can be seen in Fig. 8 that this region is excluded by the $\tilde{\tau}^+\tilde{\tau}^-$ cuts employed at high Δm. At low Δm the $\tilde{\tau}^+\tilde{\tau}^-$ signal occupies a region of the $(x_{min},\ x_{max})$ plane very similar to the $e^+e^-\ell^+\ell^-$ background; events with two identified electrons or muons must be completely or almost completely excluded from the search (see Fig. 8).

For the intermediate case, in which one lepton is identified as $e^\pm$ or $\mu^\pm$ and the other as a hadronically decaying tau, Figs. 9 and 10 show the distributions in the $(x_{e\mu}, x_{had})$ plane for Standard Model Monte Carlo and $\tilde{\tau}^+\tilde{\tau}^-$ signal events, respectively. $x_{e\mu}$ and x_{had} are the scaled momentum of the $e^\pm$ or $\mu^\pm$ and the hadronically decay-

ing tau, respectively. The cuts in x_{min} and x_{max} are shown in Fig. 10.

At the other extreme, events without identified $e^\pm$ or $\mu^\pm$ form a large fraction of the $\tau^+\tau^-$ signal, but only a small fraction of the W^+W^- background. Very loose cuts on momentum are appropriate in this case. Events in which both tau candidates have very low momentum are rejected in order to suppress the background from
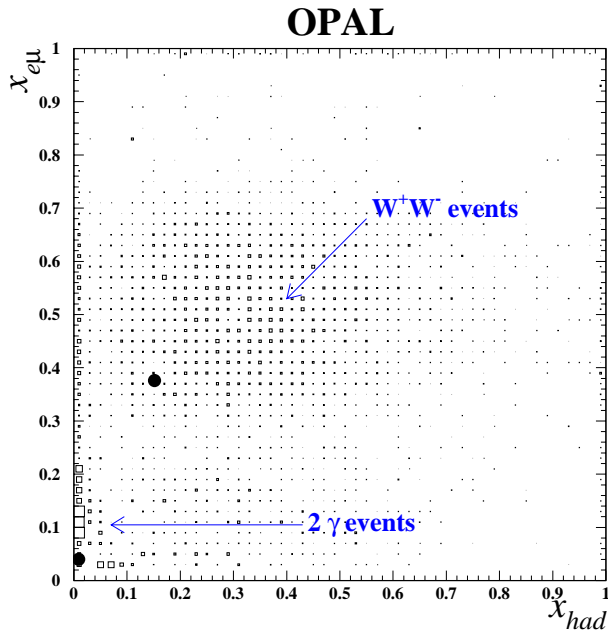
OPAL

Fig. 9. Distribution in the $(x_{e\mu}, x_{had})$ plane at $\sqrt{s} = 172$ GeV, with the requirement that one of the observed leptons is identified as $e^{\pm}$ or $\mu^{\pm}$, and the other is not. The data events are shown as the *circular points*. The Standard Model Monte Carlo distribution is shown as the *squares*. The regions that correspond to W^+W^- production and to two-photon processes are indicated
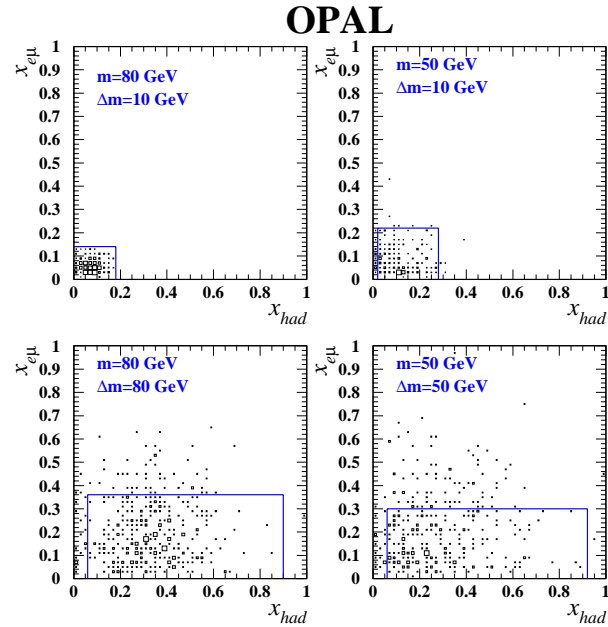
OPAL

Fig. 10. Stau Monte Carlo signal distribution in the $(x_{e\mu}, x_{had})$ plane at $\sqrt{s} = 172$ GeV, for four different combinations of $m = m_{\tilde{\tau}^-}$ and $\Delta m = m_{\tilde{\tau}^-} - m_{\tilde{\chi}_1^0}$, with the requirement that one of the observed leptons is identified as $e^{\pm}$ or $\mu^{\pm}$, and the other is not. The kinematic cuts that are applied for these values of m and Δm are illustrated

$e^+e^-\ell^+\ell^-$ events, but essentially the entire region in momentum space occupied by the signal is accepted.

4.6 Selection criteria for charged Higgs

Charged Higgs pair production can lead to acoplanar di-tau events from the decay $H^{\pm} \to \tau\nu_{\tau}$. These events would have the same properties as stau pair events for the case of massless neutralinos. The optimised kinematic cuts obtained for staus with massless neutralinos are therefore parameterised and used in the search for charged Higgs pair production. The kinematic cuts are parameterised as a 1-dimensional function of m_{H^-}.

4.7 Selection criteria for charginos

Charginos can decay to a final state containing a charged lepton and one or more invisible particles by three possible processes:

$$\text{(i) } \tilde{\chi}_1^{\pm} \to \ell^{\pm}\tilde{\nu}_{\ell},$$
$$\text{possibly followed by the decay: } \quad \tilde{\nu}_{\ell} \to \tilde{\chi}_1^0\nu_{\ell}$$
$$\text{(ii) } \tilde{\chi}_1^{\pm} \to W^{\pm}\tilde{\chi}_1^0,$$
$$W^{\pm} \to \ell^{\pm}\nu_{\ell}$$
$$\text{(iii) } \tilde{\chi}_1^{\pm} \to \tilde{\ell}^{\pm}\nu_{\ell},$$
$$\tilde{\ell}^{\pm} \to \ell^{\pm}\tilde{\chi}_1^0$$

4.7.1 Two-body chargino decay to charged lepton and sneutrino

The first case, in which the chargino decays via a sneutrino, $\tilde{\chi}_1^{\pm} \to \ell^{\pm}\tilde{\nu}_{\ell}$, is essentially a two-body decay. The observed charged lepton is produced directly in the decay of the chargino. If $\tilde{\nu}_{\ell}$ is lighter than $\tilde{\chi}_1^{\pm}$ then for a given choice of the two parameters $m_{\tilde{\chi}_1^{\pm}}$ and $m_{\tilde{\nu}}$ the lepton is mono-energetic in the chargino rest-frame. (The possible sneutrino decay is to two invisible particles and hence is unobserved.)

Efficiencies have been calculated for the case where the three sneutrino generations are mass degenerate. In this case the same di-lepton mixture is expected as for W^+W^- and for chargino decays via a W. Given the lower limits at 95% CL on the sneutrino mass from LEP1 [22] of 37.1 GeV for one sneutrino generation and 41.8 GeV for three mass degenerate sneutrinos, sneutrino masses below 35 GeV were not considered.

4.7.2 Three-body chargino decay

The second case, in which the chargino decays via a virtual or real W, $\tilde{\chi}_1^{\pm} \to W^{\pm}\tilde{\chi}_1^0 \to \ell^{\pm}\overline{\nu}_{\ell}\tilde{\chi}_1^0$, we refer to as three-body decay. The observed charged lepton is produced in the second stage of the chargino decay and its momentum spectrum is determined by the two parameters $m_{\tilde{\chi}_1^{\pm}}$ and $m_{\tilde{\chi}_1^0}$. Some kinematic distributions for two-body and three-body decay are compared in Fig. 11. It can be seen

that for a given value of m and Δm, the momenta tend to be higher for two-body decay, as would be expected because the lepton comes directly from the decay of the chargino.

The analysis applied to the three-body channel is completely analogous to the analysis applied to staus, with different kinematic cuts being applied for the three classes of two, one or zero electrons or muons being identified in the final state. Since both signal and background now involve W decay, the relative fractions of events in each of the three classes is the same for both signal and background. This was not the case for staus, and the advantage of the different fractions discussed in Sect. 4.5 is lost. The cuts on x_{max}, x_{min} are indicated in Fig. 11.

In the case of two-body chargino decays, the top left plot in Fig. 11 shows a clear need for a minimum cut on $x_{e\mu}$. This was not necessary for three-body chargino decays or staus. The application of a minimum cut on $x_{e\mu}$ (or x_{min}) is the only important difference between the analyses for two- and three-body chargino decays.

4.7.3 Two-body chargino decay via a charged slepton

Specific results for the case in which the chargino decays via a charged slepton, $\tilde{\chi}_1^\pm \to \tilde{\ell}^\pm \nu_\ell$, are not given because the kinematic distributions for the signal will depend on $m_{\tilde{\chi}_1^\pm}$, $m_{\tilde{\chi}_1^0}$ and the masses of the three charged sleptons, all of which are unknown. In general, we expect our search to be sensitive to this process. However, for particularly unfavourable choices of these masses, for example, if $\tilde{\ell}^\pm$ and $\tilde{\chi}_1^0$ are close in mass, then the final state lepton will be very soft, and events from such a decay would not be selected. Note that direct searches for charged slepton pair production are described in Sects. 4.3–4.5. All references to two-body decays in the rest of the paper refer to the $\tilde{\chi}_1^\pm \to \ell^\pm \tilde{\nu}_\ell$ decay introduced in Sect. 4.7.1.

5 Selection efficiencies, number of candidates, expected backgrounds

Tables 5–10 give the selection efficiency, the number of selected events and number of events expected from Standard Model processes of the selections for $\tilde{e}^+\tilde{e}^-$, $\tilde{\mu}^+\tilde{\mu}^-$, $\tilde{\tau}^+\tilde{\tau}^-$, H^+H^-, $\tilde{\chi}_1^+\tilde{\chi}_1^-$ (2-body decays: $\tilde{\chi}_1^\pm \to \ell^\pm \tilde{\nu}_\ell$) and $\tilde{\chi}_1^+\tilde{\chi}_1^-$ (3-body decays: $\tilde{\chi}_1^\pm \to W^\pm \tilde{\chi}_1^0 \to \ell^\pm \overline{\nu}_\ell \tilde{\chi}_1^0$), respectively. It should be noted that an individual candidate event may be consistent with a given new physics hypothesis over a range of m and Δm values. Similarly, an individual candidate event may be consistent with more than one new physics hypothesis and may, therefore, give entries in more than one of the above tables (for illustration see the rows labelled "Candidate for:" in Tables 1 and 2).

It can be seen that sizable selection efficiencies have been obtained for $\tilde{e}^+\tilde{e}^-$, $\tilde{\mu}^+\tilde{\mu}^-$ and $\tilde{\chi}_1^+\tilde{\chi}_1^-$ (2-body decays), even when Δm is as low as 2.5 GeV. Non-zero efficiencies have been obtained down to $\Delta m = 1.5$ GeV in these channels. However, in the case of $\tilde{\tau}^+\tilde{\tau}^-$ and $\tilde{\chi}_1^+\tilde{\chi}_1^-$ (3-body
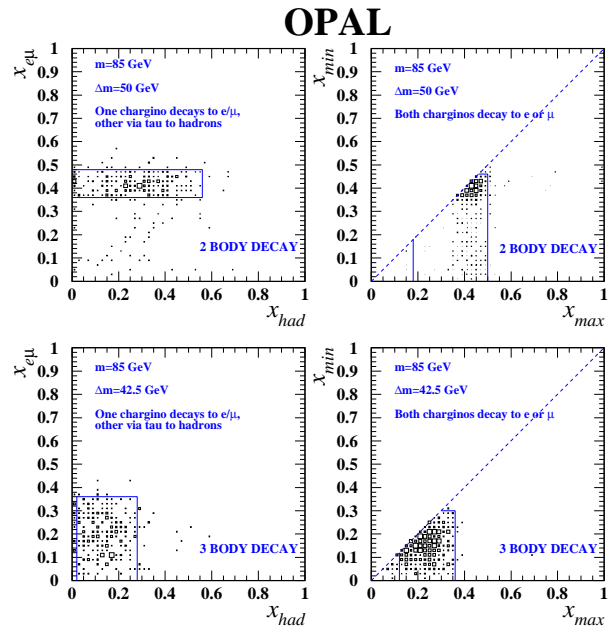

Fig. 11. Comparison between the 2- and 3-body decay hypotheses of the scaled momentum distributions of the leptons in $\tilde{\chi}_1^+\tilde{\chi}_1^-$ events. Note the need for a minimum cut on $x_{e\mu}$ for 2-body decay in the case of there being one identified electron or muon. The kinematic cuts applied for these values of m and Δm are illustrated

decays) there are additional invisible particles (neutrinos) in the final state. The visible leptons are therefore less energetic and the selection efficiencies at low Δm values are reduced.

Slepton pair efficiencies are evaluated for right-handed sleptons, both decaying to lepton and lightest neutralino $\tilde{\ell}^\pm \to \ell^\pm \tilde{\chi}_1^0$. The selectron pair events were generated at $\mu = -200$ GeV and $\tan\beta = 1.5$. The selection efficiency depends on the angular distribution of the produced selectrons and this will depend on the size of the neutralino-mediated t-channel contribution to the cross-section. We have found by varying μ and $\tan\beta$ that the above choice gives a conservative estimate of the selection efficiency.

Inefficiencies arising from random detector occupancy and other effects in the data that are not modelled in the Monte Carlo have been studied using random triggers. The most important influence of such un-modelled effects is to activate one of the "2-photon veto cuts" (cuts 6, 7 and 11 of selection I – see Appendix I). These vetoes are applied only if the event has low missing transverse momentum and so this un-modelled inefficiency is relevant mainly for events at low Δm. The selection efficiencies given in Tables 5–10 contain a correction for this effect, which amounts to a 3% reduction in efficiency for low values of Δm.

At $\sqrt{s} = 130$–136 GeV we use our previously published [17] selection efficiencies, numbers of selected events and numbers of events expected from Standard Model processes in the search for slepton and chargino pair produc-

Table 5. Selection efficiency, number of selected events and number of events expected from Standard Model processes in the search for $\tilde{e}^+\tilde{e}^-$ production at $\sqrt{s} = 161$ GeV and $\sqrt{s} = 172$ GeV for different values of $m_{\tilde{e}^-}$ and Δm. The errors are statistical only

Δm	$\sqrt{s} = 161$ GeV $m_{\tilde{e}^-}$ (GeV)			$\sqrt{s} = 172$ GeV $m_{\tilde{e}^-}$ (GeV)			
(GeV)	50	65	75	50	65	75	85
selection efficiency (%)							
1.5	5 ± 1	1 ± 0	0 ± 0	3 ± 1	1 ± 0	1 ± 0	0 ± 0
2.5	32 ± 1	29 ± 1	26 ± 1	30 ± 1	27 ± 1	23 ± 1	18 ± 1
5	57 ± 1	60 ± 1	62 ± 1	50 ± 2	52 ± 2	60 ± 2	57 ± 2
10	67 ± 1	72 ± 1	73 ± 1	63 ± 2	65 ± 2	68 ± 1	68 ± 1
$m/2$	66 ± 1	69 ± 1	67 ± 1	52 ± 2	53 ± 2	68 ± 1	68 ± 1
m	62 ± 1	71 ± 1	75 ± 1	54 ± 2	55 ± 2	74 ± 1	68 ± 1
number of selected events							
1.5	1	0	0	0	0	0	0
2.5	1	1	0	0	0	0	0
5	0	0	0	0	0	0	0
10	0	0	0	0	0	0	0
$m/2$	0	0	0	0	0	1	0
m	0	0	0	1	1	2	1
number of events expected from Standard Model processes							
1.5	0.0 ± 0.0	0.0 ± 0.0	0.0 ± 0.0	0.0 ± 0.0	0.0 ± 0.0	0.0 ± 0.0	0.0 ± 0.0
2.5	0.1 ± 0.0	0.1 ± 0.0	0.1 ± 0.0	0.2 ± 0.1	0.0 ± 0.0	0.0 ± 0.0	0.0 ± 0.0
5	0.3 ± 0.2	0.2 ± 0.1	0.0 ± 0.0	0.0 ± 0.0	0.0 ± 0.0	0.2 ± 0.1	0.1 ± 0.1
10	0.3 ± 0.1	0.0 ± 0.0	0.0 ± 0.0	0.1 ± 0.0	0.1 ± 0.0	0.0 ± 0.0	0.0 ± 0.0
$m/2$	0.4 ± 0.0	0.2 ± 0.0	0.1 ± 0.0	0.6 ± 0.0	0.4 ± 0.0	0.9 ± 0.0	0.2 ± 0.0
m	0.3 ± 0.0	0.2 ± 0.0	0.2 ± 0.0	0.6 ± 0.0	0.5 ± 0.0	1.3 ± 0.1	0.3 ± 0.0

Table 6. Selection efficiency, number of selected events and number of events expected from Standard Model processes in the search for $\tilde{\mu}^+\tilde{\mu}^-$ production at $\sqrt{s} = 161$ GeV and $\sqrt{s} = 172$ GeV for different values of $m_{\tilde{\mu}^-}$ and Δm. The errors are statistical only

Δm	$\sqrt{s} = 161$ GeV $m_{\tilde{\mu}^-}$ (GeV)			$\sqrt{s} = 172$ GeV $m_{\tilde{\mu}^-}$ (GeV)			
(GeV)	50	65	75	50	65	75	85
selection efficiency (%)							
1.5	5 ± 1	1 ± 0	0 ± 0	4 ± 1	1 ± 0	0 ± 0	0 ± 0
2.5	44 ± 2	45 ± 2	37 ± 2	31 ± 1	29 ± 1	22 ± 1	16 ± 1
5	62 ± 2	63 ± 2	62 ± 2	58 ± 2	62 ± 2	61 ± 2	60 ± 2
10	72 ± 1	71 ± 1	73 ± 1	71 ± 1	70 ± 1	72 ± 1	73 ± 1
$m/2$	79 ± 1	80 ± 1	71 ± 1	62 ± 2	67 ± 1	76 ± 1	77 ± 1
m	78 ± 1	83 ± 1	77 ± 1	63 ± 2	68 ± 1	83 ± 1	74 ± 1
number of selected events							
1.5	0	0	0	1	1	1	0
2.5	0	0	0	1	1	1	0
5	0	0	0	0	0	0	0
10	0	0	0	0	0	0	0
$m/2$	1	1	0	0	0	0	0
m	1	1	0	0	0	0	0
number of events expected from Standard Model processes							
1.5	0.0 ± 0.0	0.0 ± 0.0	0.0 ± 0.0	0.0 ± 0.0	0.0 ± 0.0	0.0 ± 0.0	0.0 ± 0.0
2.5	0.0 ± 0.0	0.0 ± 0.0	0.0 ± 0.0	0.0 ± 0.0	0.0 ± 0.0	0.0 ± 0.0	0.0 ± 0.0
5	0.1 ± 0.0	0.1 ± 0.0	0.0 ± 0.0	0.0 ± 0.0	0.0 ± 0.0	0.0 ± 0.0	0.0 ± 0.0
10	0.2 ± 0.1	0.0 ± 0.0	0.0 ± 0.0	0.1 ± 0.0	0.0 ± 0.0	0.0 ± 0.0	0.0 ± 0.0
$m/2$	0.5 ± 0.0	0.4 ± 0.0	0.1 ± 0.0	0.7 ± 0.0	0.7 ± 0.0	0.7 ± 0.0	0.2 ± 0.0
m	0.4 ± 0.0	0.4 ± 0.0	0.4 ± 0.0	0.6 ± 0.0	0.8 ± 0.0	1.5 ± 0.1	0.5 ± 0.0

Table 7. Selection efficiency, number of selected events and number of events expected from Standard Model processes in the search for $\tilde{\tau}^+\tilde{\tau}^-$ production at $\sqrt{s} = 161$ GeV and $\sqrt{s} = 172$ GeV for different values of $m_{\tilde{\tau}^-}$ and Δm. The errors are statistical only

Δm	$\sqrt{s} = 161$ GeV $m_{\tilde{\tau}^-}$ (GeV)			$\sqrt{s} = 172$ GeV $m_{\tilde{\tau}^-}$ (GeV)			
(GeV)	50	65	75	50	65	75	85
selection efficiency (%)							
2.5	3 ± 1	1 ± 0	0 ± 0	1 ± 0	0 ± 0	0 ± 0	0 ± 0
5	12 ± 1	12 ± 1	11 ± 1	13 ± 1	12 ± 1	10 ± 1	10 ± 1
10	31 ± 1	31 ± 1	23 ± 1	28 ± 1	28 ± 1	29 ± 1	29 ± 1
$m/2$	44 ± 2	51 ± 2	51 ± 2	43 ± 2	49 ± 2	51 ± 2	59 ± 2
m	50 ± 2	55 ± 2	53 ± 2	44 ± 2	47 ± 2	50 ± 2	62 ± 2
number of selected events							
2.5	1	0	0	1	1	0	0
5	1	1	0	2	1	1	1
10	2	2	0	1	1	1	2
$m/2$	1	1	1	2	2	2	2
m	1	1	1	2	2	2	3
number of events expected from Standard Model processes							
2.5	0.2 ± 0.1	0.1 ± 0.0	0.0 ± 0.0	0.2 ± 0.1	0.0 ± 0.0	0.0 ± 0.0	0.0 ± 0.0
5	0.2 ± 0.1	0.1 ± 0.0	0.1 ± 0.0	0.2 ± 0.1	0.2 ± 0.1	0.0 ± 0.0	0.1 ± 0.0
10	0.6 ± 0.2	0.5 ± 0.2	0.2 ± 0.1	0.4 ± 0.1	0.3 ± 0.1	0.2 ± 0.1	0.4 ± 0.2
$m/2$	1.0 ± 0.2	1.0 ± 0.2	0.6 ± 0.1	1.2 ± 0.2	1.4 ± 0.2	1.2 ± 0.2	1.9 ± 0.2
m	1.0 ± 0.2	1.1 ± 0.2	0.7 ± 0.1	1.3 ± 0.2	1.4 ± 0.2	1.5 ± 0.2	2.6 ± 0.2

Table 8. Selection efficiency, number of selected events and number of events expected from Standard Model processes in the search for H^+H^- in which both Higgs particles undergo the decay $H^- \to \tau^- \overline{\nu}_\tau$ at $\sqrt{s} = 161$ GeV and $\sqrt{s} = 172$ GeV for different values of m_{H^-}. The errors are statistical only

$\sqrt{s} = 161$ GeV m_{H^-} (GeV)			$\sqrt{s} = 172$ GeV m_{H^-} (GeV)			
45	55	65	45	55	65	75
selection efficiency (%)						
47 ± 2	51 ± 2	56 ± 2	35 ± 2	45 ± 2	47 ± 2	51 ± 2
number of selected events						
1	1	1	2	2	2	2
number of events expected from Standard Model processes						
0.8 ± 0.1	1.0 ± 0.2	1.1 ± 0.2	1.2 ± 0.2	1.3 ± 0.2	1.3 ± 0.2	1.5 ± 0.2

tion. For charged Higgs pair production at $\sqrt{s} = 130$–136 GeV the results given in [17] for staus in the case of massless neutralinos are used.

6 New particle search results

The number of observed candidate events and their kinematic properties are compatible with the expected background from Standard Model processes. We present limits on the pair production of charged scalar leptons, leptonically decaying charged Higgs and charginos that decay to produce a charged lepton and invisible particles. The limits are computed combining data collected at $\sqrt{s} = 161$ and 172 GeV, described in this paper, together with data previously collected at $\sqrt{s} = 130 - 136$ GeV [17].

As described in Sect. 4, the additional event selection cuts for a given search channel vary as a function of m and Δm. The number of selected candidate events (N) is calculated at each kinematically allowed point on a 0.2 GeV

by 0.2 GeV grid of m and Δm. The data at the different centre-of-mass energies are combined by simply adding the number of observed candidates. The number of expected Standard Model events (μ_B) is calculated in a similar fashion.

The 95% CL upper limit on new particle production at $\sqrt{s} = 172$ GeV, obtained by combining the data at the three centre-of-mass energies $\sqrt{s} = 130$–136 GeV, $\sqrt{s} = 161$ GeV and $\sqrt{s} = 172$ GeV is given by:

$$\sigma_{95} \cdot B^2 = \frac{N_{95}(N, \mu_B)}{\sum_i \varepsilon_i \mathcal{L}_i \omega_i},$$

where the sum runs over the three centre-of-mass energies. B is the branching ratio for the decay mode studied and the other terms are as defined[7] in Sect. 4.2.

---

[7] In the background subtraction we conservatively do not take into account the expected background at $\sqrt{s} = 130 - 136$ GeV

Table 9. Selection efficiency, number of selected events and number of events expected from Standard Model processes in the search for $\tilde{\chi}_1^+\tilde{\chi}_1^-$ (2-body decays: $\tilde{\chi}_1^\pm \to \ell^\pm \tilde{\nu}_\ell$) at $\sqrt{s} = 161$ GeV and $\sqrt{s} = 172$ GeV for different values of $m_{\tilde{\chi}_1^\pm}$ and Δm. The entries indicated by "–" correspond to a combination of $m_{\tilde{\chi}_1^\pm}$ and Δm for which no signal Monte Carlo samples were generated. Efficiencies have been calculated for the case where the three sneutrino generations are mass degenerate. The errors are statistical only

Δm (GeV)	$\sqrt{s} = 161$ GeV $m_{\tilde{\chi}_1^\pm}$ (GeV)			$\sqrt{s} = 172$ GeV $m_{\tilde{\chi}_1^\pm}$ (GeV)			
	55	65	75	55	65	75	85
selection efficiency (%)							
1.5	3 ± 1	1 ± 0	0 ± 0	3 ± 1	1 ± 0	0 ± 0	0 ± 0
2.5	17 ± 1	17 ± 1	11 ± 1	17 ± 1	18 ± 1	11 ± 1	8 ± 1
5	43 ± 2	44 ± 2	46 ± 2	42 ± 2	45 ± 2	45 ± 2	46 ± 2
10	50 ± 2	50 ± 2	53 ± 2	52 ± 2	53 ± 2	50 ± 2	54 ± 2
20	66 ± 1	68 ± 1	61 ± 2	48 ± 2	52 ± 2	58 ± 2	66 ± 2
$(m-15)/2$	$\Delta m = 20$	–	68 ± 1	$\Delta m = 20$	–	56 ± 2	67 ± 1
$m - 35$	$\Delta m = 20$	65 ± 2	72 ± 1	$\Delta m = 20$	44 ± 2	57 ± 2	71 ± 1
number of selected events							
1.5	0	0	0	1	1	1	0
2.5	1	1	0	1	1	1	1
5	1	1	1	1	1	1	1
10	0	0	0	1	1	1	0
20	1	1	0	0	1	1	0
$(m-15)/2$	$\Delta m = 20$	–	1	$\Delta m = 20$	–	2	1
$m - 35$	$\Delta m = 20$	1	2	$\Delta m = 20$	0	3	2
number of events expected from Standard Model processes							
1.5	0.1 ± 0.0	0.0 ± 0.0	0.0 ± 0.0	0.0 ± 0.0	0.0 ± 0.0	0.0 ± 0.0	0.0 ± 0.0
2.5	0.3 ± 0.1	0.1 ± 0.0	0.0 ± 0.0	0.3 ± 0.2	0.1 ± 0.0	0.0 ± 0.0	0.0 ± 0.0
5	0.5 ± 0.1	0.6 ± 0.2	0.3 ± 0.1	0.6 ± 0.2	0.4 ± 0.2	0.2 ± 0.1	0.2 ± 0.1
10	0.6 ± 0.2	0.3 ± 0.1	0.4 ± 0.2	0.9 ± 0.2	0.6 ± 0.2	0.4 ± 0.2	0.3 ± 0.1
20	1.5 ± 0.1	0.7 ± 0.1	0.2 ± 0.0	1.7 ± 0.2	1.1 ± 0.2	0.5 ± 0.1	0.3 ± 0.1
$(m-15)/2$	$\Delta m = 20$	–	0.6 ± 0.1	$\Delta m = 20$	–	1.7 ± 0.2	1.2 ± 0.2
$m - 35$	$\Delta m = 20$	1.8 ± 0.1	2.0 ± 0.1	$\Delta m = 20$	2.1 ± 0.2	3.7 ± 0.2	3.3 ± 0.2

Monte Carlo signal events are available only at certain particular values of m and Δm. The values of m range typically from $m = 45$ GeV up to $m \approx E_{\text{beam}}$ in 5 GeV steps. The values of Δm correspond to those given in Tables 5–10. Signal efficiencies at intermediate values of m and Δm are obtained by a linear 2-dimensional interpolation from the values in the tables. In addition to the Monte Carlo statistical error, we assign a 5% systematic error on the estimated selection efficiency to take into account uncertainties in the: trigger efficiency, detector occupancy, lepton identification efficiency, luminosity measurement, interpolation procedure, and deficiencies in the Monte Carlo generators and the detector simulation.

At high values of Δm the dominant background results from W^+W^- production, for which high statistics Monte Carlo samples are available that describe well the OPAL data [4,18]. In addition to the Monte Carlo statistical error, we assign a 5% systematic error on the estimated background to take into account the uncertainty in the expected W^+W^- cross-section at $\sqrt{s} = 161$ GeV (arising from the uncertainty in the measured W mass) and deficiencies in the Monte Carlo detector simulation. At low values of Δm the dominant background results from $e^+e^-\ell^+\ell^-$ events. Additional checks of the degree to which the Standard Model Monte Carlo describes these events are given at the end of Appendix I.3. The background uncertainty at low Δm is dominated by the limited Monte Carlo statistics. (As can be seen in Tables 5–10 the uncertainty is typically 20–60% at low Δm). In setting limits the Monte Carlo statistical errors and other systematics are taken into account according to the method described in [23].

Limits on production cross-section times branching ratio squared for new physics processes are now presented in a manner intended to minimise the number of model assumptions. The data at the different centre-of-mass energies have been combined by weighting the integrated luminosity according to either β^3/s or β/s which correspond to the approximate dependence on β and s of the expected production cross-section for scalars or fermions, respectively. The chosen functional forms are approximate and are used for simplicity in presenting the data. This is particularly true for processes in which t-channel exchange may be important, notably selectron pair production and chargino pair production. In these cases the cross-section dependence on centre-of-mass energy is model dependent, depending on the mass of the exchanged particle(s) and the couplings of the neutralino(s) and chargino.

Upper limits at 95% CL on the selectron pair cross-section at 172 GeV times branching ratio squared for the

Table 10. Selection efficiency, number of selected events and number of events expected from Standard Model processes in the search for $\tilde{\chi}_1^+ \tilde{\chi}_1^-$ (3-body decays: $\tilde{\chi}_1^\pm \to W^\pm \tilde{\chi}_1^0 \to \ell^\pm \nu_\ell \tilde{\chi}_1^0$) at $\sqrt{s} = 161$ GeV and $\sqrt{s} = 172$ GeV for different values of $m_{\tilde{\chi}_1^\pm}$ and Δm. The errors are statistical only

Δm	$\sqrt{s} = 161$ GeV $m_{\tilde{\chi}_1^\pm}$ (GeV)			$\sqrt{s} = 172$ GeV $m_{\tilde{\chi}_1^\pm}$ (GeV)			
(GeV)	50	65	75	50	65	75	85
selection efficiency (%)							
3	4 ± 1	3 ± 1	1 ± 0	7 ± 1	4 ± 1	3 ± 1	1 ± 0
5	16 ± 1	17 ± 1	16 ± 1	20 ± 1	18 ± 1	18 ± 1	14 ± 1
10	38 ± 2	40 ± 2	43 ± 2	36 ± 2	39 ± 2	41 ± 2	42 ± 2
20	53 ± 2	52 ± 2	52 ± 2	45 ± 2	48 ± 2	51 ± 2	56 ± 2
$m/2$	54 ± 2	61 ± 2	59 ± 2	41 ± 2	53 ± 2	53 ± 2	62 ± 2
$m - 20$	56 ± 2	64 ± 2	65 ± 2	44 ± 2	50 ± 2	49 ± 2	66 ± 1
$m - 10$	59 ± 2	61 ± 2	64 ± 2	43 ± 2	45 ± 2	49 ± 2	70 ± 1
m	56 ± 2	60 ± 2	68 ± 1	39 ± 2	42 ± 2	52 ± 2	74 ± 1
number of selected events							
3	1	0	0	1	1	1	1
5	1	1	1	1	1	1	1
10	1	1	1	1	1	1	1
20	1	0	0	1	0	0	0
$m/2$	1	1	1	1	1	1	1
$m - 20$	1	1	1	1	1	1	2
$m - 10$	2	2	1	1	1	1	4
m	2	2	2	1	1	3	5
number of events expected from Standard Model processes							
3	0.1 ± 0.0	0.0 ± 0.0	0.0 ± 0.0	0.2 ± 0.1	0.0 ± 0.0	0.0 ± 0.0	0.0 ± 0.0
5	0.5 ± 0.2	0.3 ± 0.1	0.2 ± 0.1	0.4 ± 0.2	0.2 ± 0.1	0.1 ± 0.0	0.1 ± 0.0
10	0.9 ± 0.2	0.7 ± 0.2	0.6 ± 0.2	0.7 ± 0.2	0.6 ± 0.2	0.6 ± 0.2	0.4 ± 0.2
20	1.3 ± 0.2	1.0 ± 0.2	0.6 ± 0.2	1.2 ± 0.2	0.9 ± 0.2	0.8 ± 0.2	0.7 ± 0.2
$m/2$	1.5 ± 0.2	1.0 ± 0.2	0.7 ± 0.2	1.3 ± 0.2	1.2 ± 0.2	1.1 ± 0.2	1.1 ± 0.2
$m - 20$	1.8 ± 0.2	1.6 ± 0.2	1.3 ± 0.2	1.4 ± 0.2	1.5 ± 0.2	1.5 ± 0.2	2.3 ± 0.2
$m - 10$	1.9 ± 0.2	1.8 ± 0.2	1.7 ± 0.2	1.7 ± 0.2	1.7 ± 0.2	2.1 ± 0.2	3.9 ± 0.2
m	1.9 ± 0.2	1.9 ± 0.2	1.9 ± 0.2	1.9 ± 0.2	2.2 ± 0.2	3.5 ± 0.2	6.1 ± 0.2

decay $\tilde{e}^- \to e^- \tilde{\chi}_1^0$ are shown in Fig. 12 as a function of selectron mass and lightest neutralino mass. These limits are applicable to $\tilde{e}_L^+ \tilde{e}_L^-$ and $\tilde{e}_R^+ \tilde{e}_R^-$ production. The corresponding plots for the smuon and stau pair searches are shown in Figs. 13 and 14, respectively. The data at the different centre-of-mass energies have been combined by weighting the integrated luminosity according to β^3/s.

The upper limit at 95% CL on the charged Higgs pair production cross-section times branching ratio squared for the decay $H^- \to \tau^- \overline{\nu}_\tau$ is shown as a function of m_{H^-} as the solid line in Fig. 15. The dashed line in Fig. 15 shows the prediction from PYTHIA at $\sqrt{s} = 172$ GeV for a 100% branching ratio for the decay $H^- \to \tau^- \overline{\nu}_\tau$. With this assumption we set a lower limit at 95% CL on m_{H^-} of 54.8 GeV. In a forthcoming paper [24] the search described here for acoplanar di-tau events will be combined with searches in the final states $\tau \overline{\nu} q \overline{q}$ and $q \overline{q} q \overline{q}$ to set limits on charged Higgs pair production for arbitrary $H^- \to \tau^- \overline{\nu}_\tau$ branching ratio.

The upper limits at 95% CL on the chargino pair production cross-section times branching ratio squared for the decay $\tilde{\chi}_1^\pm \to \ell^\pm \tilde{\nu}_\ell$ (2-body decay) are shown in Fig. 16. The limits have been calculated for the case where the

three sneutrino generations are mass degenerate. The data at the different centre-of-mass energies have been combined by weighting the integrated luminosity according to β/s. It should be noted that t-channel contributions are important for this case ($m_{\tilde{\nu}} < m_{\tilde{\chi}_1^\pm}$), and that the β/s approximation used for the centre-of-mass energy dependence of the cross-section can result in an under-estimate of the upper limit of up to about 20% particularly for low sneutrino masses.

The upper limits at 95% CL on the chargino pair production cross-section times branching ratio squared for the decay $\tilde{\chi}_1^\pm \to W^\pm \tilde{\chi}_1^0 \to \ell^\pm \overline{\nu}_\ell \tilde{\chi}_1^0$ (3-body decay) are shown in Fig. 17. The data at the different centre-of-mass energies have been combined by weighting the integrated luminosity according to β/s.

We can use our data to set limits on the masses of right-handed sleptons[8] based on the expected right-handed slepton pair cross-sections and branching ratios. The

---

[8] The right-handed slepton is expected to be lighter than the left-handed slepton. The right-handed one tends (not generally valid for selectrons) to have a lower pair production cross-section, and so conventionally limits are given for this (usually) conservative case
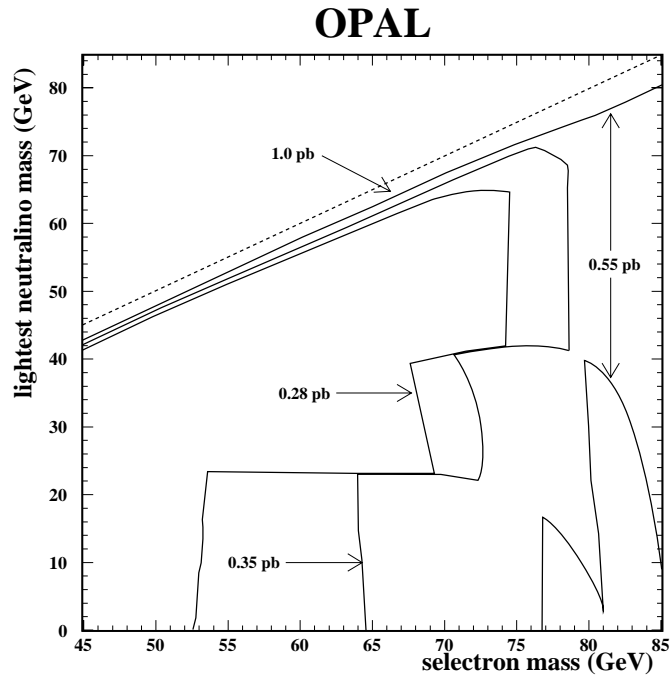
OPAL

Fig. 12. Contours of the 95% CL upper limits on the selectron pair cross-section times branching ratio squared for $\tilde{e} \to e\tilde{\chi}_1^0$ at $\sqrt{s} = 172$ GeV. The limit is obtained by combining the 130–172 GeV data-sets assuming a β^3/s dependence of the cross-section. The kinematically allowed region is indicated by the *dashed lines*
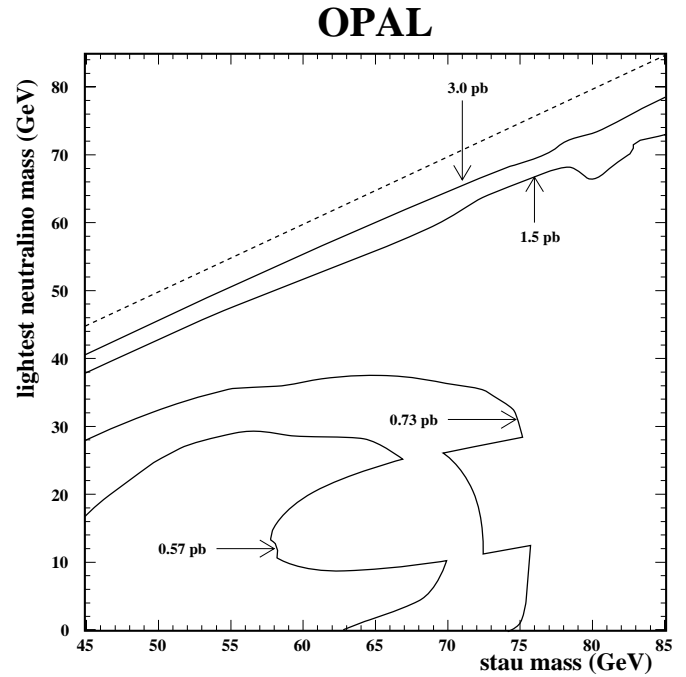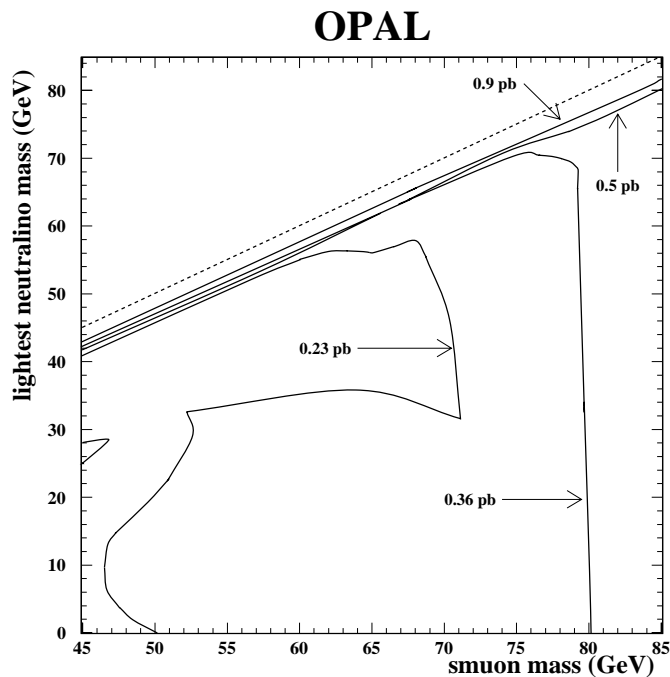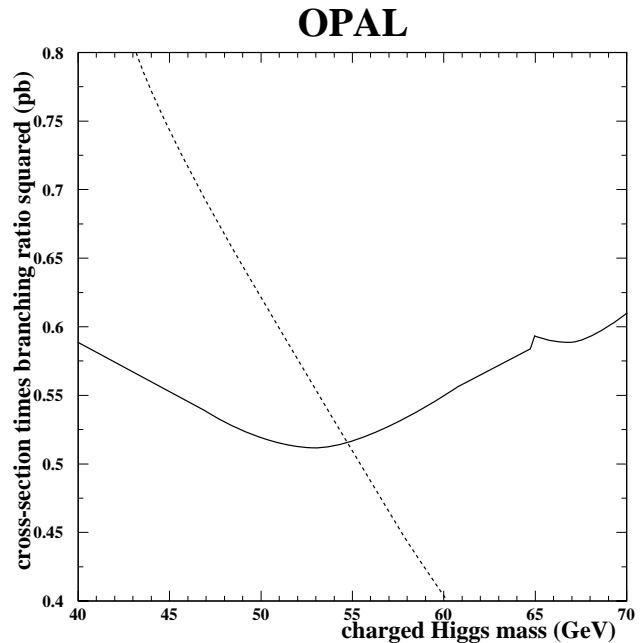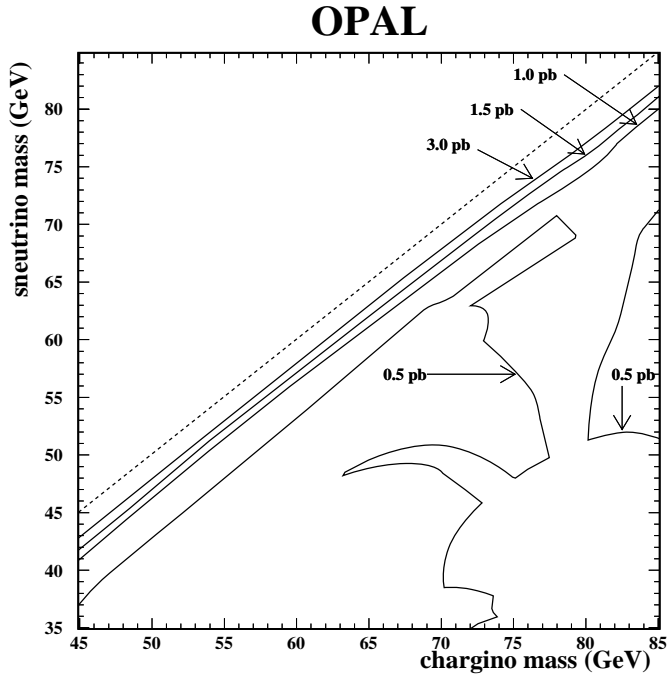
OPAL

Fig. 14. Contours of the 95% CL upper limits on the stau pair cross-section times branching ratio squared for $\tilde{\tau} \to \tau\tilde{\chi}_1^0$ at $\sqrt{s} = 172$ GeV. The limit is obtained by combining the 130–172 GeV data-sets assuming a β^3/s dependence of the cross-section. The kinematically allowed region is indicated by the *dashed lines*

OPAL

Fig. 13. Contours of the 95% CL upper limits on the smuon pair cross-section times branching ratio squared for $\tilde{\mu} \to \mu\tilde{\chi}_1^0$ at 172 GeV. The limit is obtained by combining the 130–172 GeV data-sets assuming a β^3/s dependence of the cross-section. The kinematically allowed region is indicated by the *dashed lines*

OPAL

Fig. 15. The *solid line* shows the 95% CL upper limit on the charged Higgs pair production cross-section times branching ratio squared for the decay $H^- \to \tau^-\overline{\nu}_\tau$ at $\sqrt{s} = 172$ GeV. The limit is obtained by combining the 130–172 GeV data-sets assuming the m_{H^-} and $\sqrt{s}$ dependence of the cross-section predicted by PYTHIA. For comparison, the *dashed curve* shows the prediction from PYTHIA at $\sqrt{s} = 172$ GeV assuming a 100% branching ratio for the decay $H^- \to \tau^-\overline{\nu}_\tau$
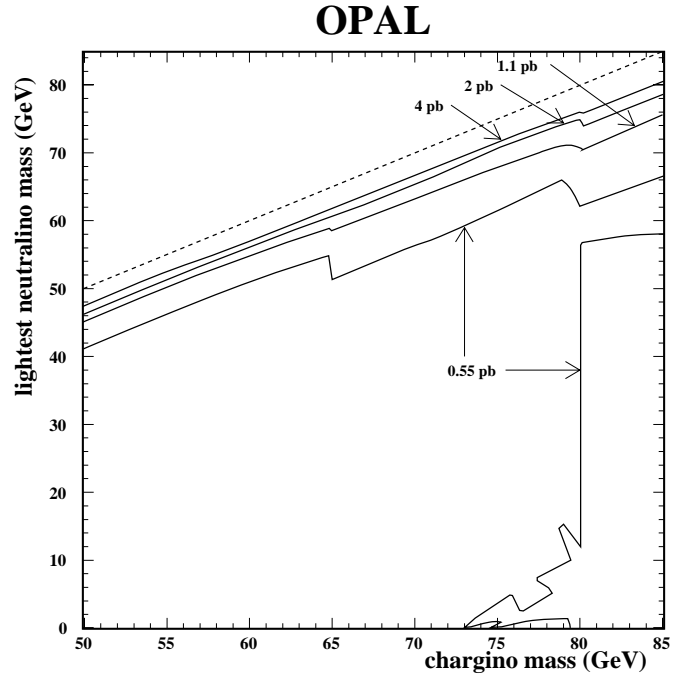
OPAL

Fig. 16. Contours of the 95% CL upper limits on the chargino pair cross-section times branching ratio squared for $\tilde{\chi}_1^{\pm} \to \ell^{\pm}\tilde{\nu}$ (2-body decay) at $\sqrt{s} = 172$ GeV. The limits have been calculated for the case where the three sneutrino generations are mass degenerate. The limit is obtained by combining the 161–172 GeV data-sets assuming a β/s dependence of the cross-section. This channel was not analysed in [17] at $\sqrt{s} = 130$–136 GeV. The kinematically allowed region is indicated by the *dashed lines*

OPAL

Fig. 17. Contours of the 95% CL upper limits on the chargino pair cross-section times branching ratio squared for $\tilde{\chi}_1^{\pm} \to \ell^{\pm}\nu\tilde{\chi}_1^0$ (3-body decay) at $\sqrt{s} = 172$ GeV. The limit is obtained by combining the 130–172 GeV data-sets assuming a β/s dependence of the cross-section. The kinematically allowed region is indicated by the *dashed lines*

cross-sections have been calculated at each centre-of-mass energy and take into account initial state radiation. The right-handed smuon pair production cross-section can be calculated from the relevant photon- and Z-exchange diagrams. The production cross-section depends simply on the smuon mass. However, the branching ratio is a function of the masses and couplings of the particles involved in open decay channels. Of particular relevance here is the $\tilde{\chi}_2^0$, which may decay to $\tilde{\chi}_1^0\gamma^{(*)}$ or $\tilde{\chi}_1^0 Z^*$ and whose mass depends on the MSSM parameters M_1, M_2, μ and $\tan\beta$. In particular regions of parameter space, the square of the branching ratio for $\tilde{\mu}_R^{\pm} \to \mu^{\pm}\tilde{\chi}_1^0$ can be essentially zero[9], and so it is not possible to provide general limits within the MSSM on smuon production on the basis of this search alone. In Fig. 18 we show limits on smuon pair production as a function of smuon mass and lightest neutralino mass for several assumed values of the branching ratio squared for $\tilde{\mu}_R^{\pm} \to \mu^{\pm}\tilde{\chi}_1^0$. The limits depend on the neutralino mass as the efficiency, number of candidates and expected number of background events vary with neutralino mass as well as the smuon mass. For a

---

[9] For example, for $M_2 = 40$ GeV, $\mu = -25$ GeV, $\tan\beta = 2$, the branching ratio squared is calculated to be 0.02 for the case of $(m_{\tilde{\mu}_R}, m_{\tilde{\chi}_1^0}) = (70, 20)$ GeV. All the quantitative predictions within the MSSM are obtained using SUSYGEN and are calculated with the gauge unification relation, $M_1 = \frac{5}{3}\tan^2\theta_W M_2$
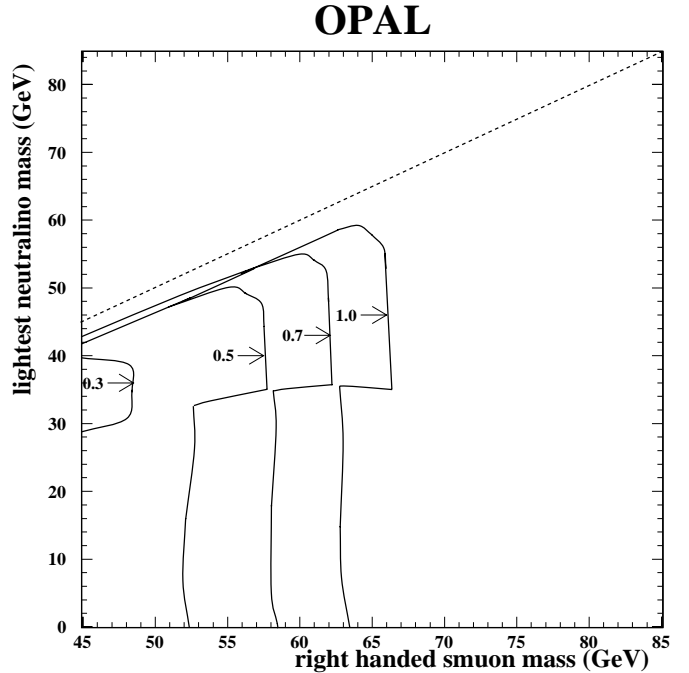
OPAL

Fig. 18. 95% CL exclusion region for right-handed smuon pair production obtained by combining the 130–172 GeV data-sets. The limits are calculated for several values of the branching ratio squared for $\tilde{\mu}_R^{\pm} \to \mu^{\pm}\tilde{\chi}_1^0$ that are indicated in the figure. Otherwise they have no supersymmetry model assumptions. The kinematically allowed region is indicated by the *dashed line*
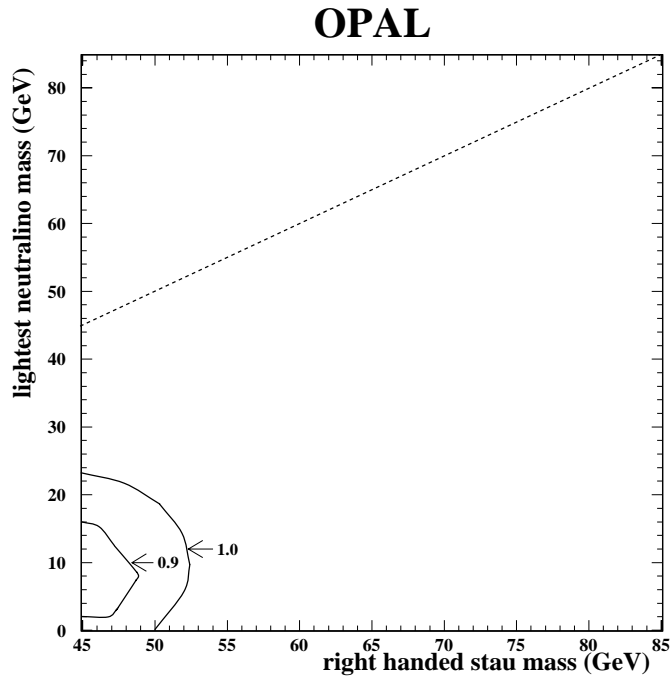
OPAL

Fig. 19. 95% CL exclusion region for right-handed stau pair production obtained by combining the 130–172 GeV data-sets. The limits are calculated for two values of the branching ratio squared for $\tilde{\tau}_R^\pm \to \tau^\pm \tilde{\chi}_1^0$. Otherwise they have no supersymmetry model assumptions. The kinematically allowed region is indicated by the *dashed line*
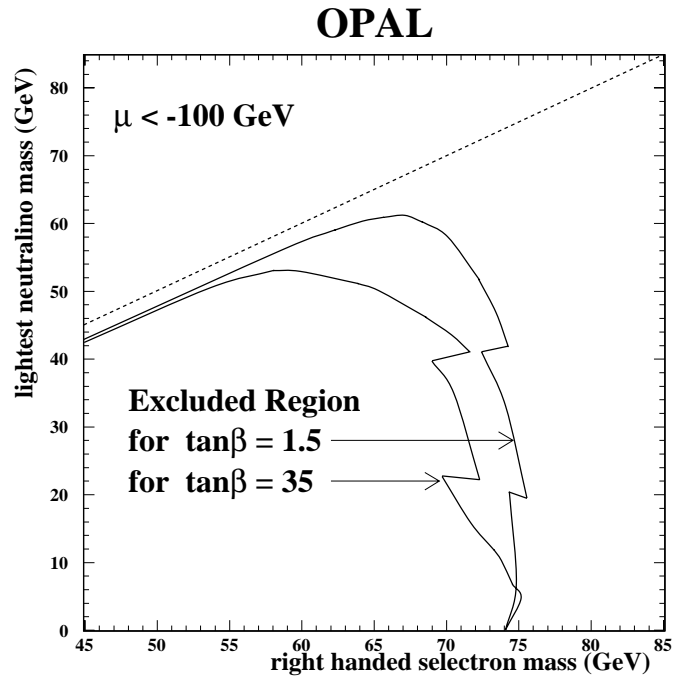
OPAL

Fig. 21. For two values of $\tan\beta$ and $\mu < -100$ GeV, 95% CL exclusion regions for right-handed selectron pairs obtained by combining the 130–172 GeV data-sets. The excluded regions are calculated taking into account the predicted branching ratio for $\tilde{e}_R^\pm \to e^\pm \tilde{\chi}_1^0$. The kinematically allowed region is indicated by the *dashed line*

OPAL
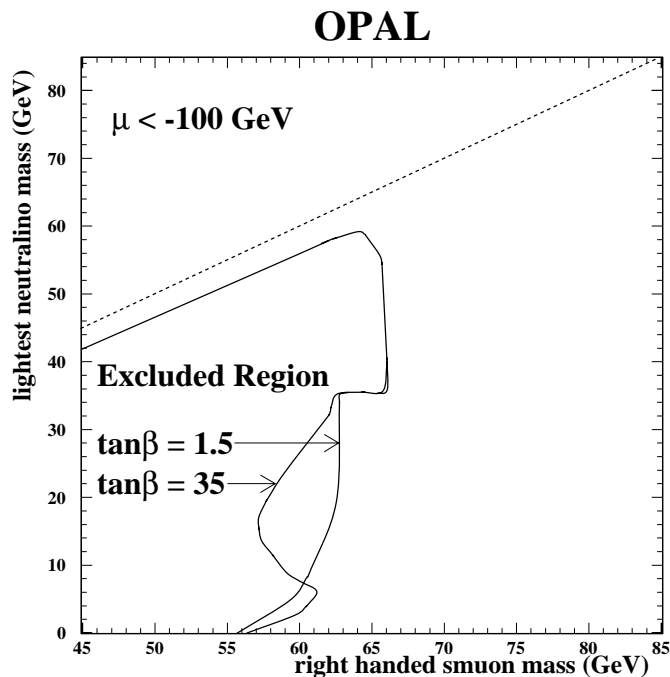
Fig. 20. For two values of $\tan\beta$ and $\mu < -100$ GeV, 95% CL exclusion regions for right-handed smuon pairs obtained by combining the 130–172 GeV data-sets. The excluded regions are calculated taking into account the predicted branching ratio for $\tilde{\mu}_R^\pm \to \mu^\pm \tilde{\chi}_1^0$. The kinematically allowed region is indicated by the *dashed line*

branching ratio $\tilde{\mu}_R^\pm \to \mu^\pm \tilde{\chi}_1^0$ of 100% and for a smuon-neutralino mass difference exceeding 4 GeV, right-handed smuon pair production is excluded at 95% CL for smuon masses below 62.7 GeV. The 95% CL upper limit on the production of right-handed $\tilde{\tau}^+\tilde{\tau}^-$ times branching ratio squared for $\tilde{\tau}_R^\pm \to \tau^\pm \tilde{\chi}_1^0$ is shown in Fig. 19. The present data-set slightly extends the limit established at LEP1.

An alternative approach is to set limits taking into account the predicted branching ratio for $\tilde{\mu}_R^\pm \to \mu^\pm \tilde{\chi}_1^0$ for specific choices of the MSSM parameters. Figure 20 shows 95% CL exclusion regions for right-handed smuon pairs in the $(m_{\tilde{\mu}_R}, m_{\tilde{\chi}_1^0})$ plane, for $\mu < -100$ GeV and for two values of $\tan\beta$ (1.5 and 35). The data at the different centre-of-mass energies 130–172 GeV have been combined by weighting the integrated luminosity according to the MSSM-predicted cross-section times branching ratio squared. For $\mu < -100$ GeV and $\tan\beta = 1.5$ and for smuon-neutralino mass differences exceeding 4 GeV, smuon masses below 55.6 GeV are excluded at 95% CL.

The right-handed selectron pair production cross-section can be enhanced significantly by the t-channel neutralino exchange diagram when the neutralino mass is small and its coupling to electron and right-handed selectron is high (gaugino-like). However due to possible interference, the cross-section may even be smaller than for smuon pair production. The presented limits are therefore quite model dependent. We have evaluated the minimum value of the expected cross-section times branching ratio squared for $\mu < -100$ GeV and for two values of $\tan\beta$

(1.5 and 35) in the ($m_{\tilde{e}_R}$, $m_{\tilde{\chi}_1^0}$) plane taking into account the production cross-section and the calculated branching ratio for $\tilde{e}_R^\pm \to e^\pm \tilde{\chi}_1^0$. The 95% CL exclusion region is shown in Fig. 21. For $\mu < -100$ GeV and $\tan\beta = 1.5$ and for selectron-neutralino mass differences exceeding 5 GeV, selectron masses below 66.5 GeV are excluded at 95% CL.

7 Summary and conclusions

A selection of di-lepton events with significant missing transverse momentum has been performed using a total data sample of 20.6 pb^{-1} at centre-of-mass energies of 161 GeV and 172 GeV. Thirteen events are observed, which is consistent with the 16.8 ± 0.5 events expected from Standard Model processes.

Further event selection criteria, in the form of kinematic cuts and lepton identification requirements, have been implemented in order to search for scalar charged lepton, charged Higgs and chargino pair production. The sensitivity to new physics has been maximised by using an algorithm to optimise the kinematic cut values as functions of the masses of the pair produced new particle and the neutral particle to which it is assumed to decay.

No evidence for new phenomena is apparent and limits on the pair production cross-section times branching ratio squared are presented for selectrons, smuons, staus, leptonically decaying charged Higgs and charginos that decay to produce a charged lepton and invisible particles. In addition, 95% CL exclusion regions in the ($m_{\tilde{\ell}_R}$, $m_{\tilde{\chi}_1^0}$) plane for selectrons, smuons and staus are presented. The limits are computed combining data collected at $\sqrt{s} = 161$ and 172 GeV, described in this paper, together with data previously collected at $\sqrt{s} = 130 - 136$ GeV [17].

With respect to our previous publications [17,25], the analysis presented here has an improved sensitivity to new physics sources of di-lepton events with significant missing transverse momentum. The results given here supersede those given in [17,25]. Model dependent limits on charged slepton pair production at LEP2 energies have been presented by the ALEPH collaboration [26].

Appendix I Event selection I

I.1 Overview

In designing the first selection particular emphasis has been placed on retaining efficiency for events with very low visible energy, but nevertheless significant missing transverse momentum. The event selection requires evidence that a pair of leptons has been produced in association with an invisible system that carries away significant missing energy and momentum. The remaining cuts reduce the probability that the signature of missing momentum is faked by Standard Model processes containing, for example, secondary neutrinos from tau decays or particles that strike regions of the detector where they are undetected or poorly measured.

At least one track in the central detector must satisfy requirements on lepton identification, isolation and momentum in the plane perpendicular to the beam axis (p_t). In order to maintain a high efficiency, especially in the region of small Δm, very much looser requirements are made on the possible presence of a second lepton in the event. A significant missing momentum is required by applying cuts on the quantities $p_t^{\text{miss}}/E_{\text{beam}}$ and $a_t^{\text{miss}}/E_{\text{beam}}$ and the angle to the beam direction of the missing momentum vector (see Sect. 3.1 for definitions).

The dominant background that survives these cuts arises from two-photon lepton pairs in which one of the electrons is scattered at a significant angle to the beam direction. Such events are suppressed by requiring no significant energy to be present in the SW and FD detectors. The inner edge of the SW calorimeter is at approximately 0.025 rad to the beam direction. A beam energy scattered electron or radiated photon can therefore carry away a p_t^{miss} of approximately $0.025E_{\text{beam}}$ and not be detected. This sets the scale for the minimum p_t^{miss} that must be required in order to suppress the two-photon background. A larger p_t^{miss} may occur without the production of a tag in SW if, for example, both beam electrons in a two-photon event are scattered at approximately the same azimuthal angle, ϕ. However, the probability for such an occurrence is rather small. Monte Carlo simulations of the Standard Model processes are used to tune the event selection cuts and to estimate the residual background. Given the above discussion, the cuts applied on p_t^{miss} and a_t^{miss} are scaled with E_{beam}. This allows the same cuts on these quantities to be applied at $\sqrt{s} = 161$ GeV and $\sqrt{s} = 172$ GeV as employed in the analysis of the data collected at $\sqrt{s} = 130$–136 GeV [17].

I.2 Lepton identification, isolation, etc.

Unless otherwise explicitly stated, tracks in the central detector and clusters in the electromagnetic calorimeter are required to satisfy the normal quality criteria employed in the analysis of Standard Model lepton pairs [27]. These criteria are as follows. Tracks must have: $p_t > 0.1$ GeV, $|d_0| < 1$ cm, $|z_0| < 40$ cm and a total of at least 20 measured points in the CV, CJ and CZ tracking chambers, the first of which is at a radius of less than 75 cm. $|d_0|$ is the point of closest approach of the track to the beam axis in the transverse plane and $|z_0|$ is the z coordinate at this point. In addition to the quality criteria of [27], tracks are required either to be matched to an ECAL cluster or to hits in CV, or to have at least 50 CJ hits.

Barrel electromagnetic clusters are considered if they have a deposited energy $E > 0.1$ GeV. Endcap electromagnetic clusters are considered if they have a deposited energy $E > 0.2$ GeV, they contain at least two blocks, and the fraction of the total energy of the cluster given by the most energetic block is less than 99%. Algorithms are adopted to avoid double-counting ECAL energy deposits associated with charged particles.

Clusters in the FD calorimeter are considered if their energy is at least 1 GeV. Clusters in the GC are con-

sidered if their energy is at least 5 GeV. Clusters in the SW calorimeter are considered if their energy is at least 1 GeV or if they are consistent with the passage of a single minimum ionizing particle through the calorimeter. An algorithm to detect short-lived noisy regions in the calorimeters is used to suppress noise clusters in EB, EE, SW, FD, GC and HCAL.

In order to suppress 'junk' events, such as those originating from beam-gas or beam-wall collisions, it is required that at least one track in the event is matched to 6 or more hits in the axial sectors of the vertex drift chamber or to an ECAL cluster with energy of at least 0.1 GeV. Events arising from the passage of cosmic ray muons through the detector are rejected using an algorithm similar to that employed in the analysis of Standard Model muon pairs [27].

A track is identified as a candidate lepton if it has $p > 1.5$ GeV and satisfies:

electron any one of the following three criteria:
1. The output of the neural network described in [28] is greater than 0.8.
2. $0.8 < E/p < 1.3$, where p is the momentum of the track and E is the energy of the associated electromagnetic cluster.
3. $0.5 < E/p < 2.0$ and $W_{dE/dx}$ is not in the range $-0.04 < W_{dE/dx} < 0.0$, where $W_{dE/dx}$ is the dE/dx weight [29] for the track to be an electron.

muon either of the following two criteria:
1. The track is identified as a muon according to the criteria employed in the analysis of Standard Model muon pairs [27]. That is, it has associated activity in the muon chambers or hadron calorimeter strips or it has a high momentum but is associated with only a small energy deposit in the electromagnetic calorimeter.
2. The track is identified as a muon according to the criteria employed in the analysis of inclusive muons in multihadronic events given in [30], with no cut on the kaon dE/dx weight.

Leptonic tau decays are usually identified as $e^{\pm}$ or $\mu^{\pm}$. Hadronic tau decays are identified as follows:

hadronic tau both of the following criteria:
1. Within a cone of half opening angle $35°$ there are no more than three tracks in total.
2. The invariant mass of all tracks and clusters within the cone is less than the tau mass (assuming the pion mass for each track).

The isolation of electron and muon candidates is defined by considering charged particles and e.m. calorimeter clusters within a cone of half opening angle $20°$ around the lepton direction. The isolation of hadronic tau candidates is defined by considering charged particles and e.m. calorimeter clusters within a cone of half opening angle $60°$, but outside the cone of half opening angle $35°$, described above. In order for a lepton candidate to be considered isolated both of the following criteria must be satisfied:

1. There are no more than two additional charged particles within the isolation cone and the sum of their momenta is less than 2 GeV.
2. There are no more than two clusters in the ECAL within the isolation cone and the sum of their energies is less than 2 GeV. (In order to minimise the sensitivity to final-state photon bremsstrahlung, if there is only one photon within the isolation cone of an electron or muon candidate it is classified as isolated irrespective of the energy of the photon.)

If a track has been identified as an electron or muon candidate, but fails the relevant isolation cuts then it is considered as a tau candidate if it satisfies the tau identification and isolation requirements given above. This is in order to retain efficiency for hadrons from tau decay that are misidentified as electron or muon candidates.

Converting photons are identified using an algorithm similar to that employed in the analysis of Standard Model muon pairs [27]. The tracks and clusters associated to the conversion are replaced by a single 4-vector representing the photon. Isolated photons are defined by requiring that there be no charged tracks within a cone of half angle $20°$ around an electromagnetic cluster or converting photon.

The 4-momenta of any tracks and clusters within the isolation cone are added to the 4-momentum of the lepton candidate.

I.3 Event selection cuts

The event selection cuts fall logically into three groups. The first group of cuts requires evidence that a pair of leptons has been produced, at least one of which must satisfy requirements on lepton identification, isolation and p_t:

1. The event must contain at least one isolated lepton candidate with $p_t > 1.5$ GeV.
2. If the event contains a second isolated lepton candidate then there must be no charged tracks other than those associated to the two lepton candidates.
   If any additional photons not associated to either of the leptons are present then the measured acoplanarity and acollinearity[10] are corrected by adding the 4-momentum of the photon to the lepton to which it is nearest in ϕ. The values $p_t^{\text{miss}}/E_{\text{beam}}$ and $a_t^{\text{miss}}/E_{\text{beam}}$ are also corrected for the presence of additional clusters.
3. If the event contains only one isolated lepton candidate and this lepton is identified as an electron or muon, the tracks and clusters not associated to the lepton are considered as a possible second lepton candidate if they satisfy the following requirements:
   (a) There is at least one additional charged track.
   (b) At least one track has $p_t > 0.3$ GeV.
   (c) The total number of additional tracks and clusters does not exceed 4.

---

[10] The acollinearity angle (θ_{acol}) is defined as the supplement of the three dimensional angle between the two lepton candidates

(d) The invariant mass of the additional tracks and clusters must not exceed the tau mass. The highest energy isolated photon in the event is excluded from this mass calculation; this is in order to retain efficiency for radiative events in which one of the leptons fails to be identified and reduces the sensitivity of the calculated efficiency to possible deficiencies in the simulation of photon bremsstrahlung.

If the event contains only one isolated lepton candidate and these requirements on the additional tracks and clusters are not satisfied then the event is rejected.

(e) If the event contains only one isolated lepton candidate and this lepton is identified as a tau then the event is rejected.

From now on the phrase "lepton candidate" will normally refer to either an isolated electron, muon or tau candidate, or the rest of the event if it satisfies the criteria 3 (a)–(d). The majority of lepton candidates identified as "tau" or "rest of event" arise from hadronic tau decays and are referred to by the symbol "h".

4. Both lepton candidates must satisfy $|\cos\theta| < 0.95$.

The second group of cuts requires evidence for the production of an invisible system that carries away significant missing energy and momentum.

5. Different cuts on the missing momentum and its direction are applied in the regions of small and large acoplanarity:

small acoplanarity $\phi_{\mathrm{acop}} < 1.2$ rad:
   (a) $p_t^{\mathrm{miss}}/E_{\mathrm{beam}} > 0.035$.
   (b) $a_t^{\mathrm{miss}}/E_{\mathrm{beam}} > 0.025$.
   (c) $|\cos\theta_{\mathrm{a}}^{\mathrm{miss}}| < 0.99$, where the direction of the missing momentum vector is calculated using the missing momentum perpendicular to the event axis in the transverse plane, $\theta_{\mathrm{a}}^{\mathrm{miss}} = \tan^{-1}(a_t^{\mathrm{miss}}/p_{\mathrm{z}}^{\mathrm{miss}})$ and $p_{\mathrm{z}}^{\mathrm{miss}}$ is the total momentum of the observed particles in the z direction.

large acoplanarity $\phi_{\mathrm{acop}} > 1.2$ rad:
   (d) $p_t^{\mathrm{miss}}/E_{\mathrm{beam}} > 0.045$.
   (e) $|\cos\theta_{\mathrm{p}}^{\mathrm{miss}}| < 0.90$, where the direction of the missing momentum vector is given by $\theta_{\mathrm{p}}^{\mathrm{miss}} = \tan^{-1}(p_t^{\mathrm{miss}}/p_{\mathrm{z}}^{\mathrm{miss}})$.

The remaining cuts ensure that the signature of missing momentum could not have been produced by Standard Model processes containing, for example, secondary neutrinos from tau decays or particles that strike regions of the detector where they are undetected or poorly measured. In a number of these cuts we look for evidence of a particle that is back-to-back in the transverse plane with the total momentum vector of the observed central detector tracks and electromagnetic clusters. The idea is that the majority of the background events have no real missing momentum in the transverse plane. If the observed tracks and clusters in such a background event appear to have a net momentum in this plane then this is due to an additional particle recoiling back-to-back to them.

6. Events with clusters in GC, FD or SW are rejected if the scaled energy, $x_{\mathrm{FDSW}} = E/E_{\mathrm{beam}}$ exceeds 0.15. Low energy, $x_{\mathrm{FDSW}} < 0.15$, GC, FD or SW clusters are used to veto the event only if they are back-to-back to within 1.2 rad with the total momentum vector of the observed tracks and clusters in the central part of OPAL. This is in order to reduce the potential loss in signal efficiency that might arise from random low energy clusters caused by possible detector noise or off-momentum electrons.

7. A new feature of the OPAL detector in 1996 is the tungsten shield that was installed to protect the central detector from radiation from the synchrotron mask. This has the potentially serious consequence of creating a hole in the SW acceptance in the angular region 0.028–0.031 rad. However, events in which a beam energy electron strikes the shield tend to yield a large number of low energy clusters in the inner edge of the endcap electromagnetic calorimeter (EE) and these can be used to provide an effective veto. For the purpose of this cut the requirements on clusters in EE are modified. Clusters are considered if they have a deposited energy of greater than 0.1 GeV and they contain at least two blocks, they are not associated to any charged track, and they satisfy $|\cos\theta| > 0.964$.

An event is rejected if it contains 3 or more such EE clusters and either of the following criteria is satisfied:
   (a) $\Delta\phi_{\mathrm{EE}} < 1.2$ rad, where $\Delta\phi_{\mathrm{EE}}$ is the acoplanarity angle between the vector sum of the momenta of the above EE clusters and the total momentum vector of the event.
   (b) The sum of the energy of all such clusters does not exceed 4 GeV.

If an event contains exactly 2 such EE clusters and both of the above criteria are satisfied the event is rejected.

8. Events containing high energy isolated photons form a potentially serious source of background, because quantities such as p_t^{miss} and a_t^{miss} may be poorly measured. However, the potential signal events may also contain isolated photons and so some care is needed in designing the selection. Events are rejected if they satisfy any of the following three criteria:
   (a) The energy of an isolated photon is greater than 25 GeV.
   (b) The number of blocks in an isolated ECAL cluster is greater than 12. If a photon strikes a part of the detector where there is a very large amount of material in front of the calorimeter the observed energy is particularly seriously degraded. In such cases the observed showers tend to be very broad.
   (c) Events with medium energy ($E < 25$ GeV) photons are examined to see whether or not the observed a_t^{miss} could have been caused by the observed photon[11]. The thrust axis in the plane perpendicular to the beam direction is calculated without including

---

[11] This cut is necessary to remove a large potential background from radiative lepton pairs, in particular radiative tau pairs

the isolated photon. If the photon lies on the opposite side of this axis to the two lepton candidates and if the p_t of the photon with respect to this axis in the transverse plane[12] is greater than that of one of the leptons then the event is rejected. In the regions $0.71 < |\cos\theta| < 0.83$ and $|\cos\theta| > 0.965$ the resolution of the calorimeter is degraded due to upstream material or poor containment. If the photon lies in one of these regions stricter requirements are applied.

9. The number of tracks passing the quality cuts given above divided by the total number of tracks reconstructed in the central detector is required to be greater than 0.2. This is in order to reject 'junk' events, such as those originating from beam-gas or beam-wall collisions.

10. The majority of Standard Model $\ell^+\ell^-$ events are coplanar and collinear. The most important cut in this analysis to remove such events is that on the value of $a_t^{\mathrm{miss}}/E_{\mathrm{beam}}$. However, in order to provide additional protection against such events, very loose cuts on acoplanarity and acollinearity are applied:

   (a) The values of ϕ_{acop} and θ_{acol} are required to exceed 0.1 rad.

   (b) If the event contains an unassociated ECAL cluster of $E > 15$ GeV then ϕ_{acop} and θ_{acol} are required to exceed 0.3 rad.

   A small residual background may arise from events in which the leptons are perfectly coplanar, but that contain a low energy cluster whose energy is overestimated by a large factor thus leading to a spuriously high $a_t^{\mathrm{miss}}/E_{\mathrm{beam}}$. In order to reject such events the cuts given above on a_t^{miss}, acoplanarity and acollinearity are applied also to those quantities calculated using the two leptons alone, i.e., without correction for the presence of unassociated photons.

11. A particularly difficult potential background originates from $e^+e^-\mu^+\mu^-$ events in which one of the electrons and one of the muons is observed and the second muon is scattered at an angle to the beam direction of less than about $\cos^{-1}(0.965)$. At such an angle the muon can carry away a significant p_t^{miss} and may thus cause the event to be selected. However, the muon is unlikely to lead to a track that passes the standard quality cuts or a cluster in FD or SW that could be used to veto the event. In order to reduce the potential background from this source, events are examined for any evidence in the muon chambers, hadron calorimeter or central detector of a muon escaping in the very forward region, back-to-back with the observed lepton pair.

12. If the charge of both lepton candidates is well measured (curvature differs from zero by more than three sigma of the measurement error) then events are rejected if both lepton candidates have a charge of $+1$ or both candidates have a charge of -1. This removes half of the remaining e – μ background from the $e^+e^-\mu^+\mu^-$ events discussed in the previous point and also other

---

[12] That is, the value of a_t of the photon

events in which one or more tracks have not been reconstructed.

Cuts 4, 6, 7, 11 and 12 are designed primarily to remove background from 2-photon processes, which produce events with relatively small missing transverse momentum. These cuts are applied only if the event has low missing transverse momentum ($a_t^{\mathrm{miss}}/E_{\mathrm{beam}} < 0.20$ for $\phi_{\mathrm{acop}} < 1.2$ rad and $p_t^{\mathrm{miss}}/E_{\mathrm{beam}} < 0.25$ for $\phi_{\mathrm{acop}} > 1.2$ rad). In addition to increasing the Monte Carlo calculated signal efficiencies, this modification also reduces the sensitivity to noise not simulated in the Monte Carlo.

We now describe some additional checks of the degree to which the Standard Model Monte Carlo describes the observed data. These checks are particularly relevant to the $e^+e^-\ell^+\ell^-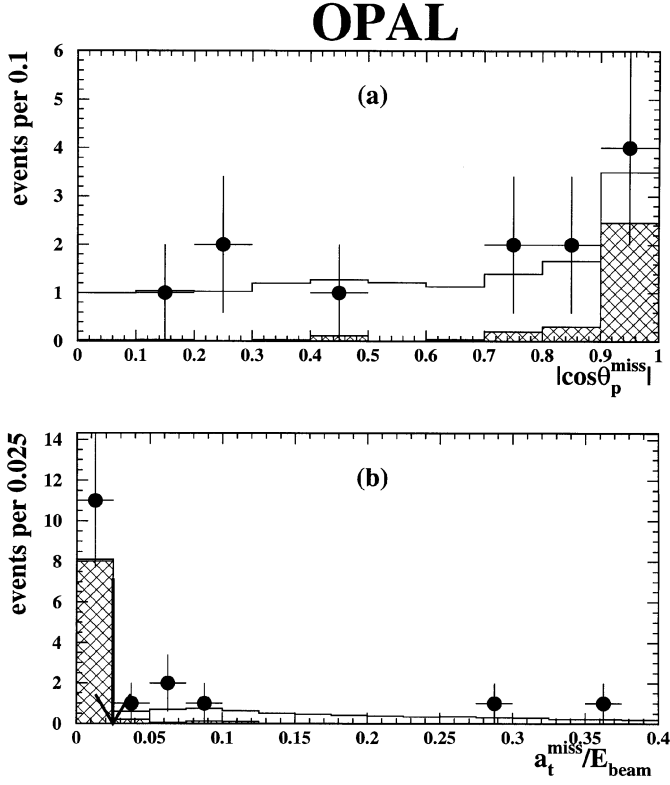$ background. Figure 22 (a) shows the distribution of $|\cos\theta_{\mathrm{p}}^{\mathrm{miss}}|$ after all selection cuts have been applied except for those on the direction of the missing momentum vector (cuts 5(c) and (e)). Figure 22 (b) shows the distribution of $a_t^{\mathrm{miss}}/E_{\mathrm{beam}}$ for events with $\phi_{\mathrm{acop}} < 1.2$ rad after all selection cuts have been applied except for that on $a_t^{\mathrm{miss}}/E_{\mathrm{beam}}$ (cut 5(b)).

As a further test of the degree to which the Standard Model Monte Carlo describes the data we relax some of the selection cuts. Cut 2 is relaxed to requiring no more than one charged track not associated to either lepton pair. Cuts 3b and 3c are relaxed to requiring no more than 6 tracks and clusters with a mass of 3 GeV. Cuts 4, 11 and 12 are removed. Cut 5 on the magnitude and direction of the missing momentum is relaxed as follows:

small acoplanarity $\phi_{\mathrm{acop}} < 1.2$ rad:
   1. $p_t^{\mathrm{miss}}/E_{\mathrm{beam}} > 0.025$.
   2. $a_t^{\mathrm{miss}}/E_{\mathrm{beam}} > 0.015$.
   3. no cut on $|\cos\theta_{\mathrm{a}}^{\mathrm{miss}}|$.
large acoplanarity $\phi_{\mathrm{acop}} > 1.2$ rad:
   1. $p_t^{\mathrm{miss}}/E_{\mathrm{beam}} > 0.035$.
   2. no cut on $|\cos\theta_{\mathrm{p}}^{\mathrm{miss}}|$.

The number of candidate events selected with these relaxed cuts at 161 GeV is 26. The number predicted by the Standard Model Monte Carlo is 30.4 ± 1.6 (stat). The number of candidate events selected with these relaxed cuts at 172 GeV is 34 and the number predicted by the Standard Model Monte Carlo is 32.1 ± 1.5 (stat). A breakdown of the Monte Carlo predicted event samples into the contributions from individual Standard Model processes is given in Table 11. Figure 23 shows the distributions of (a) $p_t^{\mathrm{miss}}/E_{\mathrm{beam}}$ and (b) $|\cos\theta_{\mathrm{p}}^{\mathrm{miss}}|$ of the events at $\sqrt{s} = 172$ GeV selected with these relaxed cuts compared with the Standard Model Monte Carlo. In all of the above checks the data and Standard Model Monte Carlo are in agreement.

I.4 W^+W^- event selection cuts

In order to suppress the contribution of Standard Model processes other than W^+W^- events some additional kinematic cuts are applied. Firstly, a loose cut is applied to

Table 11. Comparison between data and Monte Carlo of the number of events selected with the relaxed cuts given in the text. The total number of events predicted by the Standard Model is given, together with a breakdown into the contributions from individual processes. The Standard Model Monte Carlos are normalised to the experimental integrated luminosity.

$\sqrt{s}$	data	SM total	$\ell^+\ell^-$	$e^+e^-\ell^+\ell^-$	$e^+e^-q\bar{q}$	$e^+e^-Z^*/\gamma^*$	$\ell^+\nu\ell^-\bar{\nu}$
161	26	30.4	0.76	20.2	3.7	1.9	3.7
172	34	32.1	0.76	16.5	1.7	1.6	11.6

Fig. 22. (a) Distribution of $|\cos\theta_{\mathrm{p}}^{\mathrm{miss}}|$ after all selection cuts have been applied except for those on the direction of the missing momentum vector (cuts 5(c) and (e)). (b) Distribution of $a_t^{\mathrm{miss}}/E_{\mathrm{beam}}$ for events with $\phi_{\mathrm{acop}} < 1.2$ rad after all selection cuts have been applied except for that on $a_t^{\mathrm{miss}}/E_{\mathrm{beam}}$ (cut 5(b)). The position of the cut on $a_t^{\mathrm{miss}}/E_{\mathrm{beam}}$ is shown as the *arrow*. The data at $\sqrt{s} = 172$ GeV are shown as the *points with error bars*. The Monte Carlo prediction for 4-fermion processes with genuine prompt missing energy and momentum ($\ell^+\nu\ell^-\bar{\nu}$) is shown as the *open histogram* and the background, coming mainly from processes with four charged leptons in the final state, is shown as the *shaded histogram*

Fig. 23. Distributions at $\sqrt{s} = 172$ GeV of (a) $|\cos\theta_{\mathrm{p}}^{\mathrm{miss}}|$ and (b) $p_t^{\mathrm{miss}}/E_{\mathrm{beam}}$ of the events selected with the relaxed cuts described in the text compared with the Standard Model Monte Carlo. The data are shown as the *points with error bars*. The Monte Carlo prediction for 4-fermion processes with genuine prompt missing energy and momentum ($\ell^+\nu\ell^-\bar{\nu}$) is shown as the *open histogram* and the background, coming mainly from processes with four charged leptons in the final state, is shown as the *shaded histogram*

suppress the remaining background from two-photon processes and other Standard Model four-fermion events containing four charged leptons in the final state, e.g., $e^+e^- Z^*/\gamma^* \rightarrow e^+e^-\mu^+\mu^-$: events are rejected if $m_{\mathrm{recoil}} > (140\text{ GeV} + m_{\ell\ell})$. $m_{\ell\ell}$ is the reconstructed mass in GeV of the observed lepton pair and m_{recoil} is the mass in GeV of the invisible system recoiling against the lepton pair.

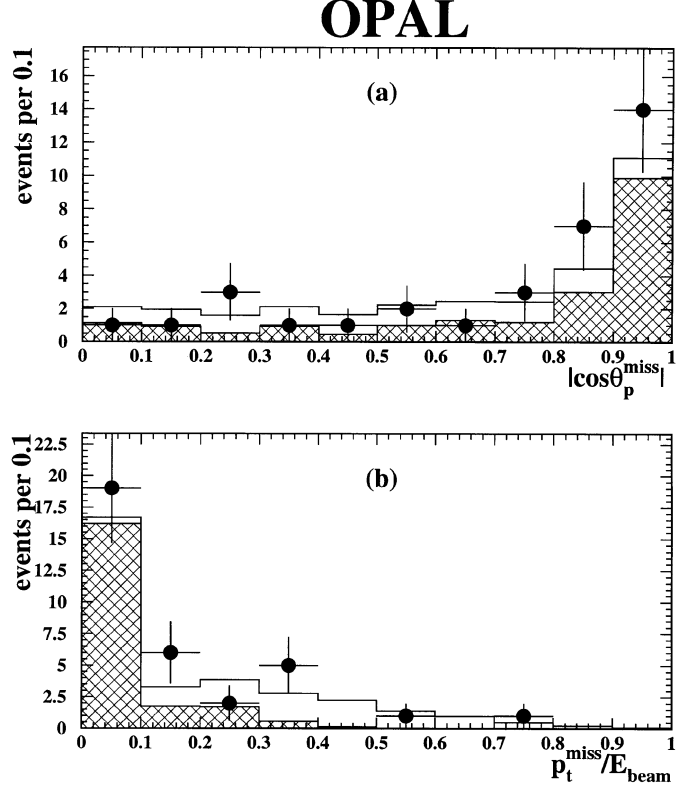The remaining cuts depend on the flavour of the observed leptons:

1. In events containing one electron and one muon (i.e., $e\mu$ events) a somewhat tighter cut against Standard Model four-fermion events containing four charged leptons is applied. If $x_{max} < 0.325$ events are rejected if $m_{\mathrm{recoil}} > (100\text{ GeV} + m_{\ell\ell})$.
2. In events containing two electrons or two muons (i.e., e^+e^-, $\mu^+\mu^-$ events) with $x_{min} < 0.325$ the recoil mass is required not to be consistent with the Z mass:
   (a) If $m_{\ell\ell} < 35$ GeV events are rejected if m_{recoil} is within 10 GeV of the Z mass.

(b) If $m_{\ell\ell} > 35$ GeV events are rejected if m_{recoil} is within 5 GeV of the Z mass.

II Event selection II

The second selection has been optimised to select and measure the rate of high visible energy events such as those from W^+W^- events in which both W's decay leptonically. Events are selected from a low multiplicity preselection [27]. It is further required that the charged track multiplicity be at least one and no more than six, and that the total number of charged tracks and clusters does not exceed twelve. Low multiplicity "jets" of charged tracks and clusters in the ECAL, GC, FD and SW calorimeters are defined using a cone algorithm [31] with a minimum energy of 2.5 GeV and a cone half angle of 20°. A separate selection is defined for jet multiplicities of one, two and three. For $W^+W^- \rightarrow \ell^+\nu\,\ell^-\overline{\nu}$ events the fraction of preselected events per jet multiplicity are 6% 1-jet, 89% 2-jet and 5% 3-jet. The former correspond mostly to events in which the decay products of one of the W's are either not reconstructed or partially reconstructed. Events naturally fall most of the time in the 2-jet category, while events with significant photon radiation observed in the detector may be classified as 3-jet events.

Electron and muon identification is applied to the most energetic track in each jet. Electrons are identified using the ratio of the energy in the ECAL to the track momentum (E/p). Tracks which are consistent with originating from photon conversions are removed, and the ionisation energy loss, dE/dx, is required to be within three standard deviations of the value expected for an electron, if there are at least 20 hits on the track with charge information. Residual background in the electron sample is removed by requiring that the track has fewer than two associated hits beyond the first two layers of the HCAL, and by requiring that the ϕ measurements of the track and ECAL cluster match to within 1°. Muons are identified as a track in the central detector which has associated hits in the muon chambers or the HCAL, and has only a small energy deposit in the ECAL. Identification of jets as electrons or muons, or as neither, is used primarily to classify events rather than as a tool for background rejection.

II.1 2-jet selection

Firstly we describe the criteria applied to all 2-jet events, and then three sets of kinematic criteria, each of which is sufficient to select the event.

II.1.1 General 2-jet criteria

D1 Both jets must contain at least one charged track and have $|\cos\theta| < 0.96$. At least one jet must satisfy $|\cos\theta| < 0.90$.

D2 The event must also have significant activity in the ECAL and in the vertex drift chamber or the silicon micro-vertex detector:

There must be at least two ECAL clusters, one of which has corrected energy exceeding 0.5 GeV. At least one of the jets must contain an ECAL cluster, and for events where no electrons or muons are identified each jet is required to contain an ECAL cluster.

Events must contain evidence for two distinct charged tracks originating from near the vertex. Either the event must contain at least two tracks reconstructed in the axial part of the vertex drift chamber or the highest energy charged track in each jet must be associated to hits in the silicon microvertex detector.

D3 The acollinearity angle of the two jets must exceed 10°.

D4 For events with $\phi_{\mathrm{acop}} > 60°$ it is required that the direction of the missing momentum satisfies $|\cos\theta_{\mathrm{p}}^{\mathrm{miss}}| < 0.95$. For events with $\phi_{\mathrm{acop}} < 60°$ it is required that $a_t^{\mathrm{miss}}/E_{\mathrm{beam}}$ exceeds 0.025, and that the direction of missing momentum calculated using a_t as described in Sect. I.3 satisfies $|\cos\theta_a| < 0.995$.

D5 Events are rejected if there are any selected tracks which are not associated with either jet.

D6 Events are rejected if a track segment in the muon chambers that is outside a 25° cone around each jet is reconstructed with $|\cos\theta| > 0.95$.

D7 The event is rejected if the maximum azimuthal separation of any two vertex chamber axial tracks exceeds 177.5°.

D8 Events with acollinearity angle less than 20° are rejected if the most energetic ECAL cluster has energy exceeding 80% of the beam energy. This criterion is used for redundancy in the rejection of Bhabha scattering events.

D9 Events with kinematic properties and identified lepton flavour similar to the $e^+e^-\mu^+\mu^-$ background are subject to further requirements. Events in which the two-jets are identified as $e-\mu$, $h-\mu$ or $h-h$, where h signifies that the jet is neither identified as an electron nor a muon, and $p_t^{\mathrm{miss}}/E_{\mathrm{beam}} < 0.25$ are considered candidates for rejection as consistent with this background source. Such events are rejected if any of the following conditions is satisfied:

[a] The net charges of both jets with associated charged tracks are non-zero and of the same sign.

[b] The least energetic jet has energy satisfying $x_{min} < 0.08$ and the electron candidate has $|\cos\theta| > 0.90$.

[c] There is a hadron calorimeter cluster reconstructed with $|\cos\theta| > 0.95$ and energy exceeding 1 GeV outside a 25° cone around each jet.

II.1.2 Kinematic criteria in selection II

Each 2-jet selection uses between two and four additional criteria based on the following five variables. Scaled variables are scaled by the beam energy. The variables are ϕ_{acop}, $p_t^{\mathrm{miss}}/E_{\mathrm{beam}}$, x_{max}, x_{min} and $m_{\ell\ell}$. Each event may

Table 12. 2-jet analysis kinematic cut values. The table lists the value of each cut quantity for each selection. Each variable is the minimum allowed value. Cuts with "–" are not applied

Cut	A	B	C1	C2	C3	C4
ϕ_{acop} (°)	5.0	15.0	5.0	15.0	5.0	5.0
$p_t^{\mathrm{miss}}/E_{\mathrm{beam}}$	0.08	0.15	0.08	0.08	–	0.08
x_{max}	$0.75-x_{min}$	–	0.30	0.20	0.30	0.30
x_{min}	0.325	–	–	–	–	–
$m_{\ell\ell}$ (GeV)	–	10.0	10.0	10.0	–	–

be selected by at most three independent selections. The values for the cut variables are detailed in Table 12.

A Kinematic selection without lepton identification. This is designed to select with high efficiency events from the e^+e^-, $\mu^+\mu^-$ and $e^\pm\mu^\mp$ classes based on kinematics without requiring lepton identification.

B Missing energy selection. This is a rather inclusive selection of all di-lepton classes based simply on significant missing transverse energy. It is required that there is at least one identified lepton (electron or muon).

C Di-lepton identification. Four mutually exclusive selections are defined depending on the lepton identification results:
C1 Di-electron or di-muon.
C2 Neither jet is identified as an electron or muon.
C3 Electron-muon.
C4 One jet is identified as electron or muon, the other is not identified as electron or muon.
The selections with at least one identified lepton require that there is at least one highly energetic jet (typically x_{max} exceeding 0.30).

II.2 3-jet selection

Events passing the preselection and classified as 3-jet events are selected if they satisfy:

T1 The number of charged tracks should be between two and four, and exactly two of the jets should contain charged tracks.
T2 The sum of the opening angles among the three 2-jet pairings should be less than 357.5°.
T3 The energy of the jet without charged tracks is added to the energy of the closest charged jet. At least one of the two jets must be identified as an electron or muon, and the total energy must exceed 30% of the beam energy.
T4 For events in which the jets are not all in one half of the transverse plane, the following criteria designed to reject $\tau\tau\gamma$ events and tagged two-photon di-lepton events are applied. The event is required to have at least one charged jet with $|\cos\theta| < 0.80$ and both must satisfy $|\cos\theta| < 0.90$. Events where the apparently neutral jet is below a polar angle at which it can be easily identified as neutral ($|\cos\theta| > 0.95$) are rejected if the energy of the neutral jet exceeds 15% of

the beam energy. An axis in the transverse plane is defined using the most energetic charged jet and the event is rejected if the transverse momentum of the neutral jet with respect to this axis exceeds 80% of the transverse momentum of the lowest energy charged jet.
T5 $p_t^{\mathrm{miss}}/E_{\mathrm{beam}} > 0.1$ and $|\cos\theta_{\mathrm{p}}^{\mathrm{miss}}| < 0.90$.
T6 The acoplanarity angle of the two charged jets should exceed 10°.
T7 Analogously to the 2-jet selection, it is also required that there must be at least two ECAL clusters, one of which has energy exceeding 0.5 GeV, and at least two tracks reconstructed in the axial sectors of the vertex chamber.
T8 Background rejection: The 2-jet selection criteria D6 and D7, the Bhabha rejection cut D8, and the like-sign rejection cut D9[a], are applied to all candidate 3-jet events.

II.3 Single-jet selection

This selection is designed for events in which one high transverse momentum lepton is observed at wide angle with evidence for a partially reconstructed lepton at small polar angle.

The single jet selection requires the following:

S1 The single jet which contains at least one charged track should satisfy $|\cos\theta| < 0.82$, be associated to an ECAL cluster and have scaled transverse momentum exceeding 0.25.
S2 The jet must be identified as an electron or muon or have ECAL energy exceeding 5 GeV.
S3 A muon track segment or ECAL or HCAL cluster should be present in the angular range $|\cos\theta| > 0.95$ and this forward activity should yield an acoplanarity angle with respect to the jet of at least 10°.
S4 Remaining background contributions, particularly from cosmic ray events are reduced to a negligible level by requiring an in time time-of-flight hit, that a track in the jet be associated to a hit in the silicon micro-vertex detector, and if two or more tracks are found in the axial part of the vertex drift chamber, that the highest azimuthal opening angle does not exceed 160°.

References

1. H.P. Nilles, Phys. Rep. **110**, (1984) 1; H.E. Haber, G.L. Kane, Phys. Rep. **117** (1985)
2. OPAL Collaboration, K. Ackerstaff et al., *"Search for Chargino and Neutralino Production at $\sqrt{s}$ = 170 and 172 GeV at LEP"*, CERN-PPE/97-083 (Submitted to Eur. Phys. J. C)
3. OPAL Collaboration, K. Ackerstaff et al., Phys. Lett. **B389** (1996) 616
4. OPAL Collaboration, K. Ackerstaff et al., Eur. Phys. J. **C1** (1998) 395
5. OPAL Collaboration, K. Ahmet et al., Nucl. Instrum. Methods **A305** (1991) 275; P.P. Allport et al., Nucl. Instrum. Methods **A324** (1993) 34; P.P. Allport et al., Nucl. Instrum. Methods **A346** (1994) 476
6. grc4f 1.0 generator: J. Fujimoto et al., KEK-CP-046, hep-ph/9603394, to be published in Comp. Phys. Comm.; J. Fujimoto et al., in *Physics at LEP2*, ed. by G. Altarelli, T. Sjöstrand, F. Zwirner, CERN 96-01, vol. 2 (1996) p. 30
7. Pythia 5.721 and Jetset 7.408 generators: T. Sjöstrand, Comp. Phys. Comm. **82** (1994) 74; LU TP 95-20
8. Excalibur generator: F.A. Berends, R. Pittau, R. Kleiss, Comp. Phys. Comm. **85** (1995) 437
9. J.A.M. Vermaseren, Nucl. Phys. **B229** (1983) 347
10. Phojet 1.05 generator: E. Budinov et al., in *Physics at LEP2*, edited by G. Altarelli, T. Sjöstrand, F. Zwirner, CERN 96-01, vol. 2 (1996) p. 216; R. Engel, J. Ranft, Phys. Rev. **D54** (1996) 4244
11. Bhwide generator: S. Jadach, W. Płaczek, B.F.L. Ward, Phys. Lett. **390** (1997) 298
12. Teegg generator: D. Karlen, Nucl. Phys. **B289** (1987) 23
13. Koralz 4.0 generator: S. Jadach, B.F.L. Ward, Z. Wąs, Comp. Phys. Comm. **79** (1994) 503
14. Nunugpv generator: G. Montagna et al., Nucl. Phys. **B452** (1994) 161
15. Susygen generator: S. Katsanevas, S. Melachroinos, in *Physics at LEP2*, edited by G. Altarelli, T. Sjöstrand, F. Zwirner, CERN 96-01, vol. 2 (1996) p. 216
16. J. Allison et al., Nucl. Instrum. Methods **A317** (1992) 47
17. "Analysis B" described in: OPAL Collaboration, G. Alexander et al., Z. Phys. **C73** (1997) 201
18. OPAL Collaboration, K. Ackerstaff et al., Phys. Lett. **B389** (1996) 416
19. OPAL Collaboration, K. Ackerstaff et al., *"Tests of the Standard Model and Constraints on New Physics from Measurements of Fermion-pair Production at 130-172 GeV at LEP"*, CERN-PPE/97-101 (Submitted to Eur. Phys. J. C)
20. J-F. Grivaz, F. Le Diberder, *"Complementary Analyses and Acceptance Optimization in New Particle Searches"*, LAL preprint 92-37, June 1992
21. *"Review of Particle Properties"*, Phys Rev. **D54** (1996), p166 formula 28.40
22. L3 Collaboration, O. Adriani et al., Phys. Rep. **236** (1993) 1
23. R.D. Cousins, V.L. Highland, Nucl. Instrum. Methods **A320** (1992) 331
24. OPAL Collaboration, *"Search for charged Higgs bosons in e^+e^- collisions at $\sqrt{s} = 130 - 172$ GeV"*, CERN-PPE/97-168 (Submitted to Phys. Lett. B)
25. OPAL Collaboration, K.Ackerstaff et al., Phys. Lett. **B396** (1997) 301
26. ALEPH Collaboration, R. Barate et al., CERN-PPE/97-056
27. OPAL Collaboration, R. Akers et al., Z. Phys. **C61** (1994) 19
28. OPAL Collaboration, G. Alexander et al., Z. Phys. **C70** (1996) 357
29. M. Hauschild et al., Nucl. Instrum. Methods **A314** (1992) 74
30. OPAL Collaboration, P. Acton et al., Z. Phys. **C58** (1993) 523
31. OPAL Collaboration, R. Akers et al., Z. Phys. **C63** (1994) 197